Heliyon 10 (2024) e29920

Contents lists available at ScienceDirect

Heliyon

journal homepage: www.cell.com/heliyon

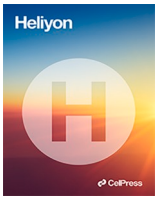

Research article

Impact of infill density on morphology and mechanical properties of 3D printed ABS/CF-ABS composites using design of experiments

Seshaiah Turaka [a], Venumurali Jagannati [b], Bridjesh Pappula [c], Seshibe Makgato [c,*]

[a] Department of Mechanical Engineering, QIS College of Engineering and Technology, Ongole, India
[b] Department of Mechanical Engineering, Annamacharya Institute of Technology and Sciences, Tirupati, India
[c] Department of Chemical & Materials Engineering, College of Science, Engineering and Technology, University of South Africa (UNISA), C/o Christiaan de Wet & Pioneer Avenue, Florida Campus, 1710, Johannesburg, South Africa

ARTICLE INFO

Keywords:
MEX
ABS
CF-ABS
Tensile
Flexural
Compressive
Izod impact
Failure mechanisms
Taguchi analysis
HR-SEM

ABSTRACT

Metal Extrusion (MEX) is a leading 3D printing technology for polymers, enabling intricate designs and personalized products in various applications. The current study evaluate how infill density affects the tensile, flexural, compressive, Izod impact and fracture behaviour of Acrylonitrile Butadiene Styrene (ABS) and Carbon Fiber Reinforced-Acrylonitrile Butadiene Styrene (CF-ABS) specimens manufactured using the MEX method. Different infill densities of 20, 40, 60 and 80 % are used in the production of honeycomb infill pattern samples for investigating the mechanical as well as fracture behaviour of MEX ABS/CF-ABS components. The experimental runs of fabricated composites were tested using a digital Izod impact tester and servo-controlled hydraulic universal testing machine, following ASTM standard procedures. The experimental findings show that CF-ABS specimens with an 80 % infill density and honeycomb fill pattern showed significant improvements in tensile strength, modulus, yield strength and elongation. The flexural strength (64.74 %), flexural modulus (209.15 %), compressive strength (125.21 %), compressive modulus (108.34 %) and impact strength (38.91 %) of these specimens are comparable to those of 3D printed ABS specimens and other infill densities. The research shows that precise management of processing variables can greatly improve the mechanical properties of 3D-printed ABS samples, providing valuable insights for a range of applications.

1. Introduction

Additive manufacturing, referred to as 3D printing, has rapidly advanced across various industries such as automotive, electronics, aerospace and medical applications [1]. Among the various 3D printing technologies for polymers, Metal Extrusion (MEX) has emerged as a leading method, offering the ability to create intricate designs and personalized products with ease. MEX, also known as Fused Filament Fabrication (FFF), which involves the extrusion of thermoplastic filament being heated and layering material to build 3D components [2]. This technique is favored for its versatility, cost-effectiveness and the wide range of available materials [2,3]. However, MEX can be prone to defects like inter-bead porosity, particularly due to limitations in the circular nozzle deposition process [3]. Nevertheless, MEX is being widely adopted in aerospace, automotive and consumer product industries for producing structural components. Cress and colleagues propose that in the coming decade, polymers produced through MEX will replace various traditional

* Corresponding author.
E-mail address: makgato2001@yahoo.com (S. Makgato).

https://doi.org/10.1016/j.heliyon.2024.e29920
Received 20 February 2024; Received in revised form 17 April 2024; Accepted 17 April 2024
Available online 23 April 2024

designs [4]. A variety of polymers, such as polyetherimide, thermoplastic polyurethane, polyethylene, and others, are notably used in MEX processes [2]. FDM has limits in porosity, surface quality, form accuracy and welding quality [5]. Layer-by-layer deposition may cause porosity, compromising structural integrity and exterior resistance [6]. Due to visible layer lines, MEX may yield rough surface finishes that need post-processing to improve appearance [7]. Dimensional errors and warping may affect form accuracy during printing, affecting complicated geometries and overhanging parts [8].

The current study selected Acrylonitrile Butadiene Styrene (ABS) and Carbon Fiber-Reinforced Acrylonitrile Butadiene styrene (CF-ABS) from a variety of polymers. ABS as well as CF-ABS are both used in the automotive industry to produce interior components, dashboard parts, trim pieces, and vehicle parts; in the aerospace industry-lightweight parts, drone frames, brackets and structural parts; and rapid prototyping functional parts-housings, brackets, gears and enclosures for various devices and machinery [1,3]. ABS and CF-ABS exhibit distinct performance characteristics in thermal and mechanical analyses. ABS is renowned for its outstanding mechanical qualities; yet its use in the production of thin components has been restricted owing to its relatively low melt fluidity. Despite this drawback, the impact resistance, strength, and stiffness of ABS make it a popular choice in engineering thermoplastics [9]. Recent investigations have focused on the mechanical, thermal and physical characteristics of ABS in additive manufacturing [9]. On the other hand, CF-ABS, a ceramic matrix composite with a notable degree of specific stiffness, thermal shock resistance and fracture behaviour [10]. Both ABS as well as CF-ABS are highly effective materials in 3D printing technology, enabling the manufacturing of a diverse array of products for different applications across various fields. 3D printing has seen rapid development across various industrial applications, like aerospace, automotive, electronics and medical fields [11]. Despite its wide range of applications, MEX 3D printers often produce specimens with subpar mechanical properties, limiting their use in structural components and reducing the technique's overall appeal.

Researchers have mostly focused on improving the mechanical qualities of printed items by analyzing the impact of processing parameters [12,13]. For example, Nabavi-Kivi et al. [13] found that increasing the printing speeds and using larger fracture angles improved the characteristics of dog bone and semi-circular bending samples. In their study, Shahbaz et al. [14] looked at how layup configurations and tip-notch radii affected the brittle fracture behaviour of 3D-printed ABS specimens. Khosravani et al. [15] demonstrated that the tensile strength of open-hole plates can be significantly improved compared to Poly Lactic Acid (PLA) specimens. Agarwal [16] highlighted the impact of layer thickness as well as print speed on enhancing tensile properties in ABS specimens. Panagiotis et al. [17] utilized expanded perlite microspheres as filler in extrusion processes to create ABS composite filament for 3D printing, showing that a 20 % granulometry improved crushing resistance. Brackett et al. [18] found that increasing infill percentage and layer thickness resulted in higher elastic modulus and ultimate tensile strength. Abeykoon et al. [19] concluded that infill density and speed played significant roles in improving ABS specimens. In the end, Cicero et al. [20] showed that graphene-ABS samples had much better mechanical properties than pure PLA and ABS.

The mechanical properties of ABS material that is 3D printed have been investigated by numerous researchers. The findings indicated that the orientation of the raster (30°, 45° and 60° angles) and the thickness of each layer have a notable impact on the mechanical characteristics [21–23]. The mechanical properties increase with the increase in layer thickness and feed rate [24–27]. Other factors, such as building orientation, nozzle sizes as well as layer thickness, also affect the mechanical characteristics [28,29]. Thermo-mechanical characteristics of ABS 3D-printed specimens also improve with lower void density and limited filament orientation [30]. Researchers have compared ABS and PLA samples using artificial aging techniques, finding that ABS samples respond more to chemical changes than PLA samples exposed to UV radiation and temperature [31]. Studies on TPU blends in ABS material reveal that adding 10–20 wt% of TPU improves adhesion between layers without lowering yield strength [32]. Researchers have found that adding a supplementary heating plate to the printing head of a MEX 3D printer increases tensile strength and ductility [33].

MEX has been utilized to produce 3D-printed cylindrical parts with enhanced ductility, increased mechanical characteristics and increased sphere wall thickness [34–36]. Rodríguez-Reyna et al. [37] optimized 3D printed components using MEX technology, focusing on tensile strength, infill pattern, and ABS's intrinsic characteristics for optimal fatigue behaviour, resulting in extended lifespans and optimal stiffness [38]. Karupaiah et al. [39] found that ABS has a higher water absorption rate than CF/ABS due to hydrophobic properties. Incorporating carbon fiber enhances vibration characteristics, increasing natural frequencies and damping ratio in three-dimensional printed composites [39,40]. Petousis et al. [41]'s study on 3D-printed ABS parts found that layer thickness emerged as the main controlling parameter, whereas the nozzle temperature and raster deposition angle exhibited comparatively lower levels of significance. Vidakis et al. [40]'s study examined the influence of six control factors on 3D printed item quality indicators, revealing that mechanical properties generally improve after specific recycling cycles, with optimal behaviour observed during the third to fifth repeat [42,43]. Parpala et al. [44] investigated the influence of infill density as well as infill line width on natural frequency using numerical simulation models and a finite element script. Dudescu et al. [45] investigated the effects of infill patterns, printing directions, and infill rates on the mechanical characteristics of 3D printed components. Do et al. [46] 's study found a strong correlation between printing patterns and compressive strength in MEX 3D printing structures, with infill density significantly affecting these properties.

The detailed literature review summarizes several research studies focused on improving the mechanical qualities of ABS 3D-printed items by analysing the impact of various processing parameters. Researchers have examined factors such as printing speed, crack angles, tip-notch radii, layup configurations, infill density, layer thickness, building orientation, nozzle sizes, void density and filament orientation. Studies have shown that these parameters significantly influence characteristics such as tensile strength, fracture resistance, flexural strength, impact strength, ductility and vibration characteristics. However, the literature review reveals a gap in understanding how to improve mechanical properties through raster angle, layer thickness and fibre volume fraction, highlighting the need for optimization of infill density with different filament materials. The objective of this study is to utilize experimental testing and Taguchi's mixed flow L_8 array optimization technique to optimize input process parameters like infill density, honeycomb pattern, and

materials, while maintaining constant printing speed and layer height. The Taguchi mixed flow L_8 array optimization technique was employed to maintain constant input process parameters like infill density, honeycomb pattern and materials, while determining strain rate sensitivity per polymer material. This study explores the influence of infill densities, infill pattern, and build direction on the tensile, compressive, flexural, hardness, and Izod properties of ABS as well as CF-ABS 3D printed composites. Additionally, SEM morphology was utilized to inspect the failure mechanisms of both ABS and CF-ABS under various mechanical loads.

2. Materials and methods

2.1. Materials and printing parameters

ABS and CF-ABS 3D printing filaments (dia. of 1.75 mm) were obtained from Think Robotics, New Delhi, India. It exhibits a melting temperature of 230 °C, a density of 1.11 g/cm^3, an average molecular weight of 100–750 g/mol, a melting flow rate of 8 g/10 min at 230 °C and a 2.26 kg load. Tables 1 and 2 present the properties and 3D printing parameters of the ABS and CF-ABS thermoplastic filaments.

Carbon fibre was selected as a stabilizer to improve the mechanical characteristics of ABS in several factors like increased strength, improved stiffness, enhanced tensile strength, reduced weight, better thermal properties and dimensional stability, making them suitable for wide range of applications. Print speed, nozzle temperature, infill pattern, and infill density were selected based on their significant influence on the qualities of the MEX 3D printed component, as explored in the existing literature [22,31]. The chosen parameters are described concisely as follows.

2.1.1. Infill density

Infill density is the amount of material used for the inner section of a printed part, which is deposited using the STL model [32]. The selection of infill densities in 3D printing depends on the several factors like strength requirement, weight consideration, cost and time constraints, part functionality, printing constraints and material properties for the intended application. Depending on the needs of the application, the infill density can be set between 10 % and 100 %. Typically, it is adjusted within a range above 50 % to evaluate its impact on different responses [33]. Nevertheless, it is possible to reduce the range if the component is designed for visual or experimental reasons to conserve the filament.

2.1.2. Infill pattern

Infill patterns are interior designs used to bulk fill 3D-printed components, including zig-zag, hexagon, linear, triangular, and other [34]. The honeycomb, trihexagonal, and triangular designs are the most often used among the various options. The honeycomb pattern, which has a hexagonal cell arrangement, creates a strong, lightweight material with enhanced mechanical properties due to its uniform distribution of stress and strain.

2.2. Design of experiment

Taguchi's experimental design involves employing OAs to arrange the factors that impact the process and determine the appropriate levels in which the variables could be adjusted. In contrast to the factorial design, the Taguchi approach evaluates a pair of options rather than considering all possible combinations. This methodology aids in gathering data to understand factors affecting product quality, reducing trials, thereby resulting in cost and time savings. The process parameters were assigned a pair of variables as well as two mixed levels, as indicated in Table 2. Based on practical experience, specimens are fabricated with infill density levels ranging from 20 % to 80 %.

The infill density with honeycomb pattern used in this study as honeycomb structures are efficient at minimizing surface area because they use hexagonal, which are packed together tightly without wasting space. This allows for optimal use of the material while providing strength and stability. Other filled patterns have irregular shapes or leaves caps between cells, resulting in an increased surface area and less material usage. The melting temperature for ABS and CF-ABS, as recommended by the filler material manufacturer, is 230 °C and 240 °C [6]. The temperatures needed for printing ABS and CF-ABS materials vary due to the inclusion of carbon fibres (CFs) in CF-ABS. The CFs have different thermal properties as compared to ABS material, requiring hot temperatures for proper melting and adhesion during the printing process. In addition, that CF-ABS typically requires high temperatures to ensure proper flow and bonding of the carbon fibre-infused material, resulting in improved strength and stiffness in the 3D printed parts. Other studies have also adapted similar levels and parameters [30,32,33]. The test samples were printed using the MEX 3D printer CreatBot@F430

Table 1
The mechanical characteristics of filament materials made of ABS and CF-ABS [35].

Properties	Unit	CF-ABS	ABS
Ultimate Tensile Strength	Mpa	22.1–57.0	22.1–46.00
Tensile Modulus	GPa	1.01–5.26	1.00–1.65
Tensile Elongation	%	3.0–19.0	3.0–17.00
Flexural Strength	MPa	42.0–76.5	42.0–70.50
Flexural Modulus	GPa	1.00–5.26	1.00–2.70

Table 2
Parameters for ABS and CF-ABS specimen 3D printing input [40].

Parameters	CF-ABS	ABS
Nozzle Diameter (mm)	0.4	0.4
Printing speed (mm/s)	45	45
First layer height (mm)	0.35	0.35
First layer speed (mm/s)	10	10
Extruder temperature (°C)	24	230
Extrusion width (mm)	0.4	0.4
Extrusion multiplier	1	1
Bed temperature (°C)	90	90
Fan speed (%)	35	35
Internal/external fill pattern	Honeycomb	Honeycomb
Infill percentage (%)	20, 40, 60 and 80	20, 40, 60 and 80

plus desktop MEX 3D printer 400x (Henan Creatbot Tech. Ltd., Zhengzhou, China). The studies were conducted using an L_8 OA Taguchi design.

2.3. Fabrication of 3D printed specimens

The printer features a brass nozzle with a diameter of 0.4 mm. The procedure was executed at a nozzle temperature of 230 °C, a bed temperature of 90 °C, a filament layer thickness of 0.32 mm, and a printing speed of 45 mm/min. The choice of 3D printing settings involves a thorough analysis of various factors, including material type, printer model, layer height, printing speed, infill density, support structures, temperature settings, build plate adhesion, cooling settings and post-processing. The specimens were made horizontally using a hexagonal infill pattern (shown in Fig. 1) and a raster angle of approximately 45 °C between the layers. The infill density was 20, 40, 60 and 80 %. The Prusa Slicer Software (2.5.2 version) generated the G-Codes for the extrusion nozzle tool paths. Fig. 2 shows the process for fabricating and testing the 8 samples.

2.4. Compressive, flexural, tensile and izod impact testing procedures

Mechanical testing was conducted on ABS and CF-ABS specimens using the ASTM D638 [47], ASTM D790 [48], ASTM D695 [49] and ASTM D256 [50] standards to assess and determine their characteristics. In accordance with the criteria, a total of five samples were prepared for every group to ascertain the material properties. Additionally, a total of 160 samples were produced for the purpose of conducting a CF-ABS filament with 20 % loading would contain 20 % CFs by weight and 80 % ABS testing, to rationalize with the CF/ABS broader goals of additive industrial innovation, driving manufacturing processes and product development.

The specimens utilized for universal hydraulic tensile testing possess a cross-sectional shape resembling that of a dog bone, with dimensions of 165 × 19 × 3.2 mm. UTM BISS Instron 8502 (capacity 25 KN) was employed with 1 mm/min strain displacement rate. The tensile strength and the modulus of elasticity were calculated using Eqs. (1) and (2) as per Ref. [38].

$$F_{ut} = \frac{P_{max}}{A} \tag{1}$$

where P_{max} = maximum load before failure (N), F_{ut} = ultimate tensile strength (MPa) and.
A = average cross-sectional area (mm^2).

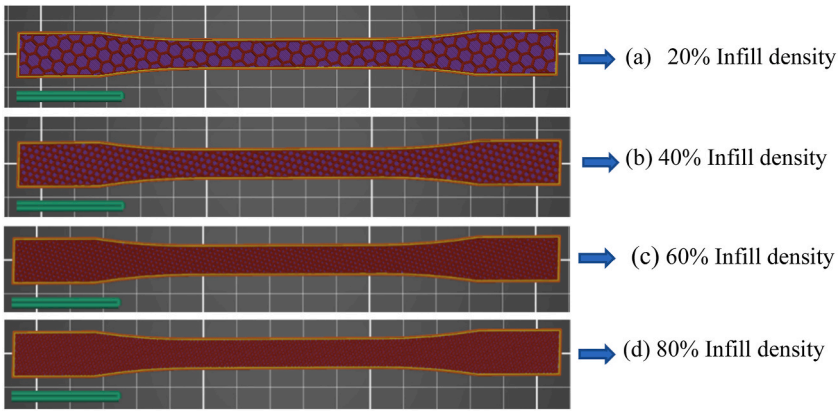

Fig. 1. Schematic graphical representation of honeycomb (hexagonal) pattern and orientation with respect to the ABS and CF-ABS specimens.

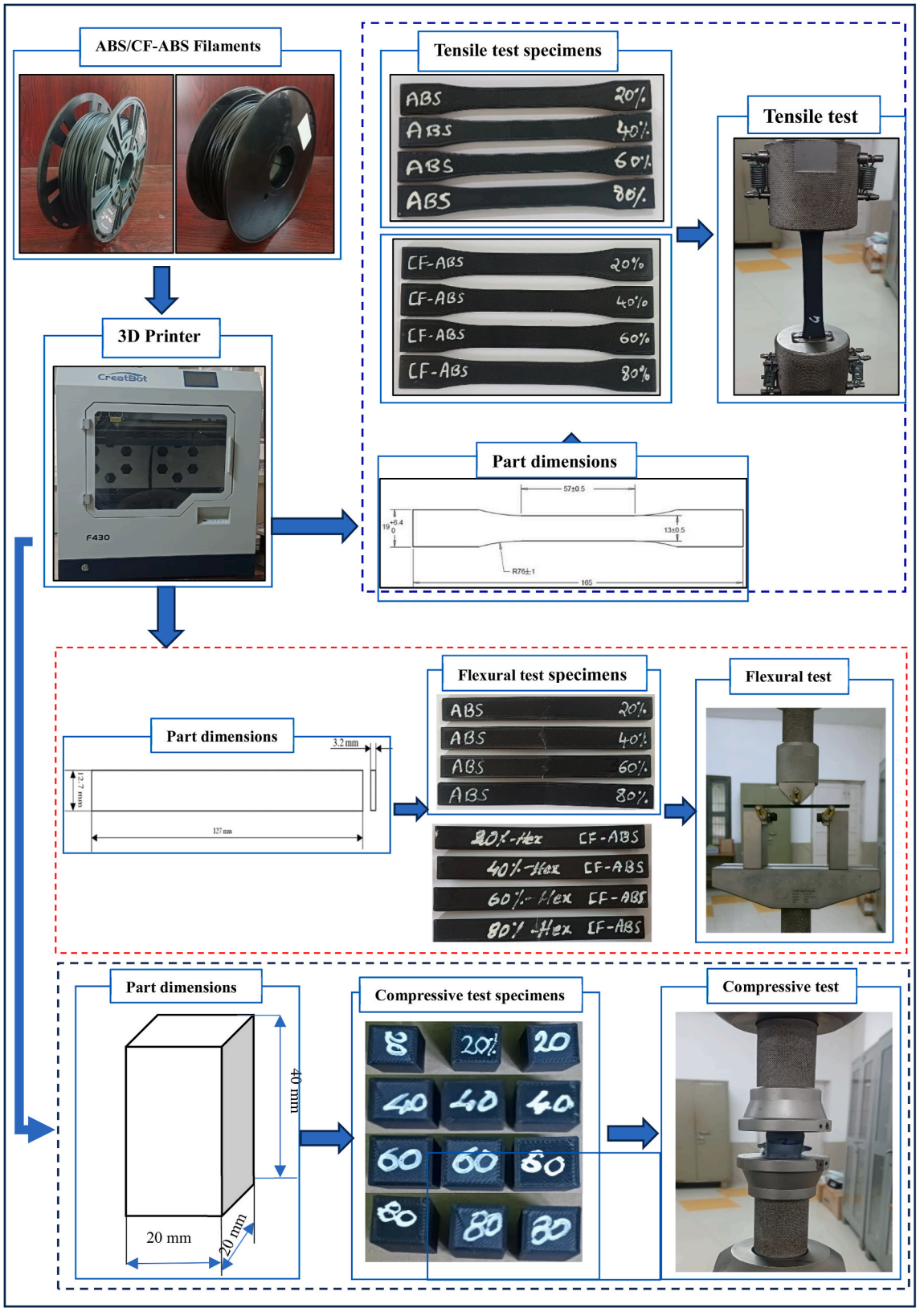

Fig. 2. The fabrication of ABS/CF-ABS specimens in accordance with ASTM standards and the experimental testing procedure.

$$E = \frac{\Delta\sigma}{\Delta\epsilon} \tag{2}$$

Where $\Delta\sigma$ = difference between applied tensile stress at two points, $\Delta\epsilon$ = difference between the two strain points and E = Young's modulus (GPa). The applied load, $\Delta\sigma$ and associated elongation, $\Delta\epsilon$ or strain of the specimens measured during the test were used to estimate the Young's modulus.

The samples used for the flexural testing were produced with specifications of 127 × 12.7 × 3.2 mm. In accordance with the ASTM D790, a total of five samples were prepared for both ABS and CF-ABS. A flexural or 3-point bending configuration, consisting of two supports and a centrally applied load nose with a diameter of 10 mm, was set up for the purpose of conducting a 3-point bending test using the BISS UTM. The flexural test was accomplished with a cross head feed rate of 1 mm/min and a span support length of 80 mm. The data acquisition software, BISS was utilized to gather measurements of flexural force (expressed in Newtons) and strain displacement (measured in millimetres). The flexural stress as well as flexural modulus of elasticity were estimated by employing Eqs. (3) and (4) correspondingly [38].

$$\sigma_F = \frac{3PL}{2bd^2} \tag{3}$$

where P = Load applied at the mid-point on the specimen (N), L = Length of the span (mm), b = width of the specimen (mm), σ_F = Flexural stress (N/mm^2) and d = depth of the specimen (mm).

$$E_F = \frac{(\sigma_{F2} - \sigma_{F1})}{(\epsilon_{F2} - \epsilon_{F1})} \tag{4}$$

where σ_{F2} and σ_{F1} are the flexural stresses, ϵ_{F2} and ϵ_{F1} are the flexural strains at the specified location on the load-deflection curve, E_F is the flexural modulus (GPa)

For compressive testing, the cuboid samples were produced with the specifications of 20 × 20 × 40 mm. As per ASTM D695, five specimens were fabricated for each ABS and CF-ABS. Compressive set-up was established for the compressive testing using BISS UTM. The compressive test was conducted using a cross-head feed rate of 1 mm/min. To measure the compressive modulus, an extensometer was mounted to the front of the specimen. Data acquisition was done using BISS software collecting the compressive force (N) and strain displacement (mm). The compressive stress and compressive modulus were estimated using Eqs. (5) and (6) respectively [31].

$$F_c = \frac{P_{max}}{A} \tag{5}$$

Where, F_c = Maximum compressive strength (MPa), P_{max} = maximum compressive load before failure (N), A = minimum cross-sectional area (mm^2).

$$E_c = \frac{\Delta\sigma}{\Delta\epsilon} \tag{6}$$

where, E_c = Compressive modulus (GPa), $\Delta\sigma$ = Difference in applied compressive stress between two strain points, $\Delta\epsilon$ = difference between the two strain points.

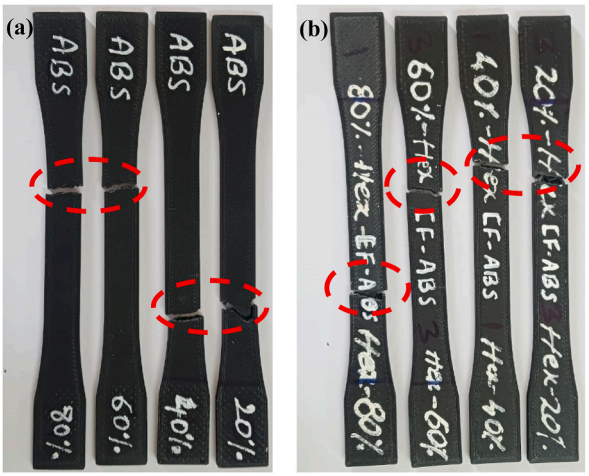

Fig. 3. Fractured specimens after performing tensile tests: (a) ABS-20, 40, 60, and 80 %; (b) CF-ABS-20, 40, 60, and 80 %.

2.5. Fracture morphology of the specimens

After performing mechanical tests on the samples, we examined the fracture morphology using a SEM, FEI-Quanta FEG 200F, equipped with a Schottky emitter. The imaging software, specifically FEI-Quanta Elements 5.5.1.00, was utilized for preparing and analysing the data at a magnification of 20×. This was done to examine the user interfaces among the deposited layers, and the distinct and cracked fibres (CF-ABS) within the matrix. These analyses were conducted after conducting the tensile as well as the flexural tests. A single specimen was selected from each of the five tested specimens of each infill density for analysis of the morphology of the fracture interface.

3. Results and discussion

3.1. Tensile test properties

The tensile test was conducted to evaluate and contrast the tensile properties of the ABS and the CF-ABS samples. For each group of infill density, Fig. 3 shows the fractured specimens after the test. Fig. 3(a) depicts ABS-20, 40, 60, and 80 %, while Fig. 3(b) depicts CF-ABS-20, 40, 60, and 80 %. Increasing the infill densities clearly led to a decrease in gaps within the composite structures, thereby enhancing the cross-sectional areas capable of effectively bearing tensile loads [43].

Table 3 presents the results of the L8 array experiment conducted on the tensile properties of ABS and CF-ABS using the Taguchi mixed level DOE. Two different composite configurations, ABS as well as CF-ABS were examined experimentally. The tensile strength of ABS as well as CF-ABS specimens showed a progressive improvement as the infill density increases from 20 % to 80 %. It can also be found that the tensile strength for ABS and CF-ABS is increased by 15.86 %, 10.59 %, 6.8 % and 9.02 % at 20, 40, 60 and 80 %, respectively. As a result of this trend, higher infill densities should result in a more compact internal structure [43]. This will improve the material's mechanical properties and make it less likely to deform when stretched. Nevertheless, the correlation between infill density and the rate of improvement in tensile strength is found to be more significant for CF-ABS composites as compared with pure ABS [18]. This finding implies that the impact of CFs on reinforcement becomes more pronounced as the infill density increases. This enhanced performance could be ascribed to the elevated strength-to-weight ratio and rigidity of CFs, which reinforce the polymer matrix and enhance its ability to bear loads [44].

The tensile test is a fundamental mechanical technique used to understand and characterize material behaviours, providing crucial insights into their mechanical properties and being a cornerstone in materials research and engineering. It can also be found that the tensile strength for ABS and CF-ABS is increased by 15.86 %, 10.59 %, 6.8 % and 9.02 % at 20, 40, 60 and 80 %, respectively. The increase in infill density results in a greater deposition of material during the printing process, hence causing a more compact internal structure within the composite component [43,44]. By increasing the density of infill, the number of voids between printed layers decreases, resulting in a more even distribution of reinforcement materials and a decreased likelihood of faults that could compromise the strength of the structure. The incorporation of CFs in CF-ABS composites serves to enhance reinforcing and enhance the overall strength of the composite material. The observed improvement in tensile strength is further ascribed to the synergy amidst the reinforcing material and the matrix. The highest tensile strength recorded from the study is 36.922 Mpa for CF-ABS with 80 % infill density. The ductility values of CF-ABS composites exhibit a modest increase compared to pure ABS composites across all infill densities. This observation implies that the inclusion of CFs has a beneficial influence on the elastic properties of the composites. CFs, renowned for their exceptional strength-to-weight ratio as well as the rigidity, have the potential to enhance the overall flexibility of the composite material, resulting in slightly elevated ductility values in comparison to pure ABS [12]. Nevertheless, the difference in ductility between ABS and CF-ABS composites is comparatively less pronounced when compared to the observed difference in tensile strength. The inclusion of CFs in composites with varying infill densities demonstrates a notable improvement in the yield strength when compared to composites made solely of ABS [32]. These findings indicate that the addition of CFs to ABS matrix enhances the material's overall strength, resulting in increased resistance to plastic deformation and improved yield strength. This observation suggests that the presence of denser internal structures enhances the load-bearing capacity and resistance to deformation [36]. In contrast, the correlation between infill density and yield strength in pure ABS composites is not uniform, as certain infill densities (such

Table 3
Results of L_8 array of the Taguchi mixed level DOE for tensile test

Run	Input parameter		Output parameter				
	Infill density (%)	Filament material	Composite code	Tensile strength (MPa)	Young's modulus (GPa)	Ductility (%)	Yield strength (MPa)
1	20	ABS	20 ABS	18.432 ± 0.84	0.434 ± 0.04	2.022 ± 0.42	20.133 ± 0.02
2	20	CF-ABS	20 CF-ABS	21.342 ± 0.42	0.853 ± 0.01	2.153 ± 0.89	22.272 ± 0.01
3	40	ABS	40 ABS	23.264 ± 0.76	1.261 ± 0.04	2.394 ± 0.44	26.231 ± 0.04
4	40	CF-ABS	40 CF-ABS	26.021 ± 0.81	1.682 ± 0.14	2.431 ± 0.28	29.242 ± 0.03
5	60	ABS	60 ABS	27.993 ± 0.71	0.464 ± 0.04	4.271 ± 0.72	21.746 ± 0.08
6	60	CF-ABS	60 CF-ABS	30.049 ± 0.84	0.892 ± 0.03	4.653 ± 0.96	24.051 ± 0.02
7	80	ABS	80 ABS	33.590 ± 0.92	1.386 ± 0.06	4.792 ± 0.94	28.853 ± 0.04
8	80	CF-ABS	80 CF-ABS	36.922 ± 1.24	1.932 ± 0.08	4.894 ± 0.98	33.621 ± 0.06

as 20 % and 60 %) demonstrate comparatively lower yield strength values. The observed variability in the printed part can be ascribed to various causes, including interlayer adhesion and the existence of voids or flaws. At an infill density of 80 %, the CF-ABS composite exhibits a significantly greater yield strength (33.621 MPa) compared to the pure ABS composite (28.853 MPa). The combination of CF reinforcement and increased infill densities has a synergistic effect on improving the mechanical characteristics of the composites.

3.1.1. Ultimate tensile strength

The results in Fig. 4(a) show that ABS had a lower ultimate tensile strength (UTS) when it had a honeycomb-type infill pattern at 20 % infill density than when it had 80 % infill density, which was 26.021 MPa. Either a less robust honeycomb lattice configuration or an increased presence of more void spaces within the 3D-printed honeycomb-type filled pattern can explain the phenomenon. This led to lower cohesive forces, which caused the UTS to drop when compared to infill densities that were higher [44,45].

The Fig. 4(b) shows that the UTS of CF-ABS at 80 % infill density using the honeycomb pattern was 36.922 MPa, which is a lot higher than that of ABS, which was 26.021 MPa. This is a 41.89 % increase. The observed phenomenon is attributable to the availability of carbon layers for adhesion or bonding with the adjacent carbon layers. This, in turn, resulted in an increase in the amount of material utilized for side-build printing and a subsequent enhancement in the tensile strength [31]. Furthermore, a greater amount of matrix material becomes available for adhesion, leading to an increase in infill density and subsequent improvements in tensile potency [27].

3.1.2. Tensile modulus or Young's modulus

Fig. 5 shows the Young's modulus of ABS and CF-ABS samples with various infill densities and honeycomb-shaped infill patterns. The findings from Fig. 5(a) indicate that the ABS material with a honeycomb-type infill pattern and 20 % infill density exhibited a lower tensile modulus of 0.434 GPa in comparison to the 80 % infill density, which showed a value of 1.682 GPa. According to the data,

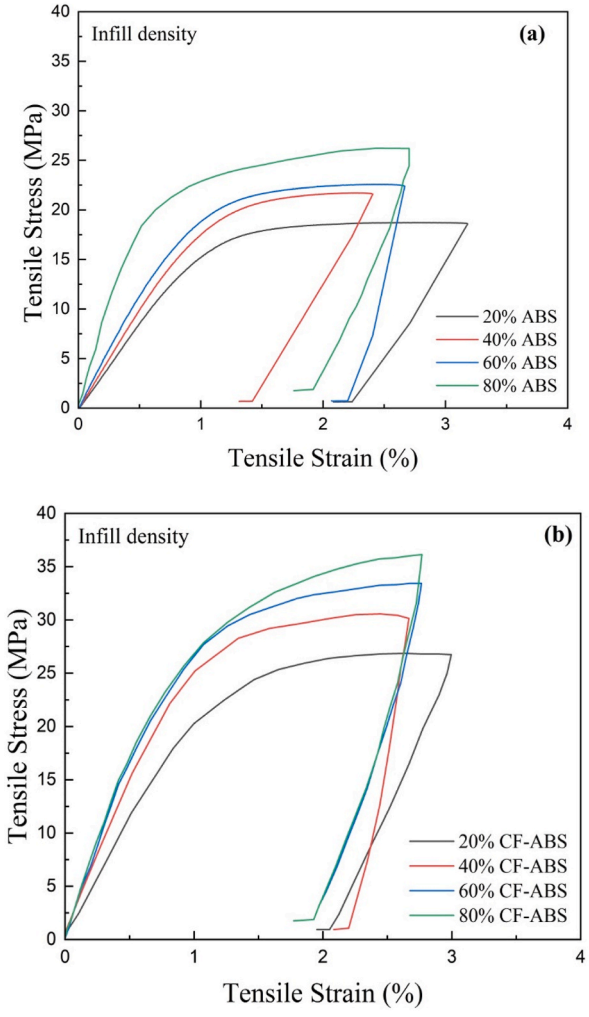

Fig. 4. A Tensile stress-strain curves for (a) ABS and (b) CF-ABS.

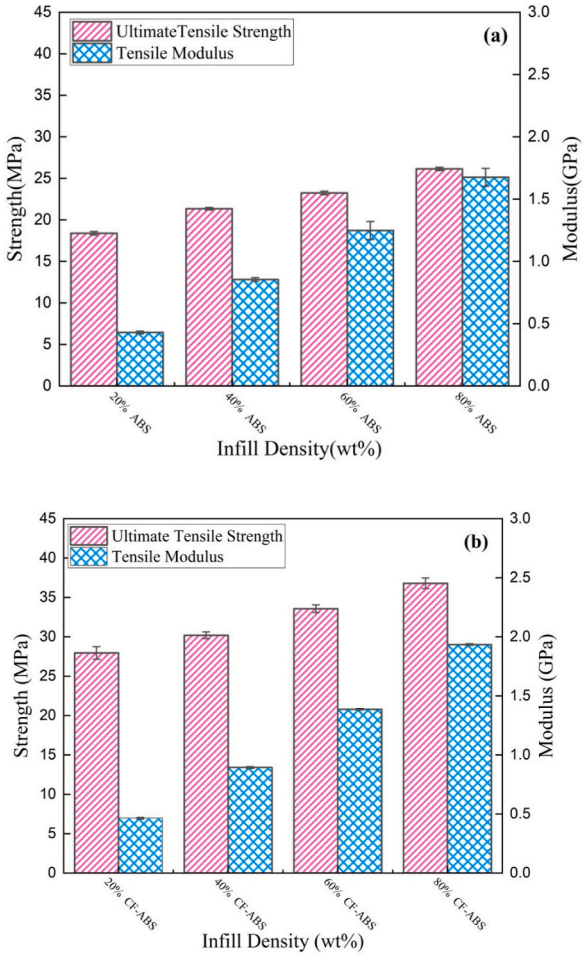

Fig. 5. Tensile strength Vs tensile modulus for varying infill density along with honeycomb type infill pattern (a) ABS and (b) CF-ABS.

the infill density of 20 % with a honeycomb-type fill pattern exhibits the lowest resistance to plastic deformation when compared to other infill densities. Fig. 5(b) shows that the CF-ABS material, filled with a honeycomb-shaped pattern and a density of 80 %, exhibited the highest tensile modulus of 1.932 GPa. In comparison, the ABS material displayed a tensile modulus of 1.682 GPa, which is significantly lower. Specifically, the CF-ABS material demonstrated an increase of 14.97 % in tensile modulus, 54.61 % in yield strength, and 101.31 % in elongation compared to the ABS. Fig. 5(b) depicts a plot graph that shows an increase in infill density, which in turn leads to a proportional increase in the tensile modulus for all 3D-printed specimens. The observed phenomenon can be attributed to the robust interlayer bonding of carbon filaments, facilitating not only the interface bonding of adjacent carbon layers but also enhancing the efficacy of heat treatment, ultimately leading to an enhanced tensile modulus [28].

3.1.3. Elongation or ductility

The ABS and CF-ABS 3D-printed specimens, subjected to various infill densities and honeycomb-type infill pattern types, exhibit elongation or ductility in Fig. 6. The observations in Fig. 6(a) suggest that the elongation of ABS with a honeycomb-type infill pattern at 20 % infill density was comparatively lower at 2.022 % than that of 80 % infill density at 4.894 %. The underlying cause is that a low infill density results in a porous structure that generates numerous sites within the material where failure may occur. Based on the results shown in Fig. 6(b), CF-ABS with a honeycomb-type infill pattern and 80 % infill density had the highest elongation of all the samples tested, at 4.894 %. In comparison, ABS exhibited an elongation rate of 2.431 %. The significant levels of deformation exhibited by the specimens' strain values, along with their ability to withstand the stress resulting from the imposed load, may explain the observed phenomena [28].

3.1.4. Main effects plots for tensile test

The main effects plots (Figs. 7–10) represent the influence of infill density with honeycomb pattern over the UTS, tensile modulus, ductility and yield strength of ABS and CF-ABS. This finding suggests that both parameters have significant influence, but there is a slight reduction in the tensile properties such as strength, modulus, ductility and yield strength of ABS filament material were

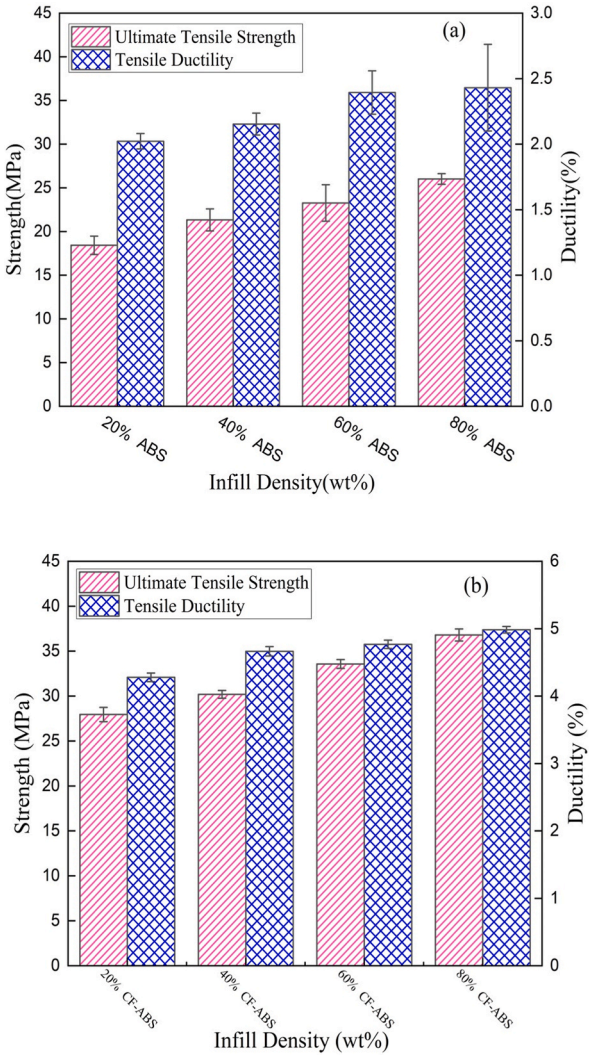

Fig. 6. Tensile strength vs. tensile ductility for varying infill density along with honeycomb-type infill patterns (a) ABS and (b) CF-ABS.

maintained at constant nozzle temperature 230 °C. The maximum tensile properties were achieved for CF-ABS filament material at 80 % infill density for honeycomb pattern and its parts were maintained at constant nozzle temperature (240 °C) and print speed (45 mm/s) [45,46].

3.2. Flexural test response of ABS and CF-ABS

The flexural test was executed to compare the flexural strength as well as the flexural modulus of 3D-printed specimens for each group of infill density and honeycomb-type patterns. Fig. 11 displays the fractured specimens following the flexural test. Fig. 11(a) depicts the fracture behaviour of specimens after compressive test response for ABS, while Fig. 11(b) depicts the fracture behaviour of CF-ABS. The flexural test's validity, as per the ASTM D790 standard, is contingent on the condition that the maximum strain within the outermost part of specimen failure falls within the prescribed 5 % strain limit. The present investigation observed that none of the specimens fractured beyond the imposed strain limit of 5 %. Table 4 presents the experimentally obtained values of flexural strength and flexural modulus.

Table 4 illustrates how infill density affects flexural strength differently based on the composite type. CF-ABS composites consistently show improved strength with higher infill densities, indicating denser internal structures enhance load-bearing capacity. Despite a general correlation between higher infill densities and increased strength, occasional declines occur, likely due to factors like interlayer adhesion and flaws. Incorporating CFs notably enhances flexural strength, especially with higher infill densities [51]. For instance, at 80 % infill density, CF-ABS composite strength (128.423 MPa) significantly surpasses that of pure ABS (105.911 MPa), highlighting the synergistic effect of CF reinforcement and increased infill densities on the mechanical properties.

The inclusion of CFs in composites significantly improves flexural modulus compared to pure ABS, indicating enhanced strength

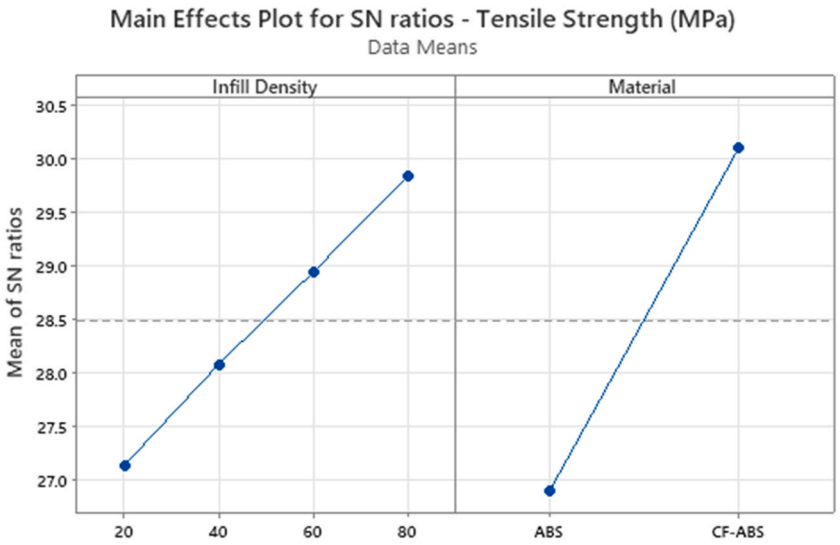

Fig. 7. Main effects plot for tensile strength Vs infill density for ABS and CF-ABS materials.

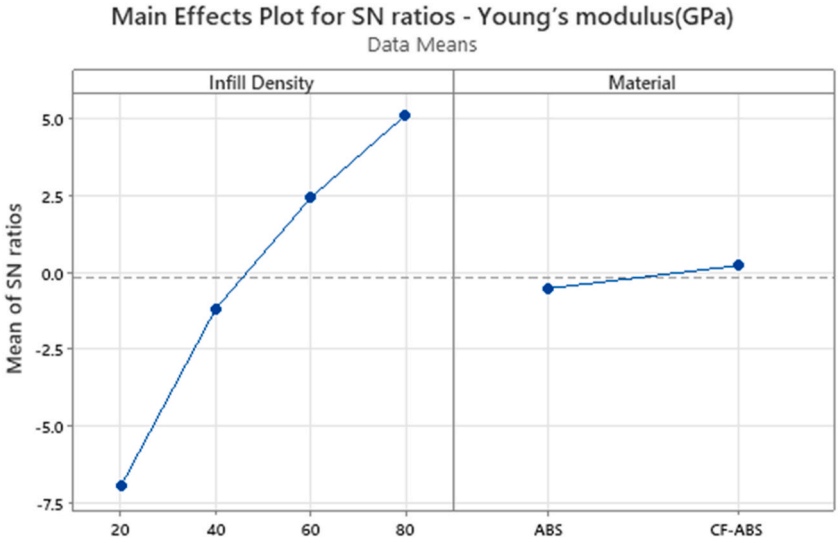

Fig. 8. Main effects plot for Youngs modulus Vs infill density for ABS and CF-ABS materials.

and rigidity [52]. For CF-ABS composites, increasing infill densities consistently enhances flexural modulus, while the relationship for pure ABS is less straightforward due to factors like interlayer adhesion and voids. The comparison of flexural modulus values among various composite codes reveals a notable enhancement resulting from the use of CFs, particularly when larger infill densities are employed [51,52]. At a density of 80 % infill, the flexural modulus of the CF-ABS composite (7.361 GPa) exhibits a significant increase in comparison to the pure ABS composite (6.278 GPa). The combination of CFs reinforcement with increased infill densities enhances the stiffness and mechanical characteristics of the composites, demonstrating a synergistic effect.

The effect of infill density on flexural strain varies depending on the composite type. CF-ABS composites show consistent improvement in flexural strain with increasing infill densities, indicating denser structures enhance flexibility. However, in pure ABS composites, the correlation between infill density and flexural strain is inconsistent, with occasional decreases observed. Factors like interlayer adhesion and voids contribute to this variability. The CFs reinforcement significantly enhances flexural strain, especially at higher infill densities. For instance, at 80 % infill, CF-ABS exhibits higher flexural strain (4.691 %) compared to pure ABS (4.135 %), indicating synergistic enhancement of flexibility and ductility.

3.2.1. Flexural stress-strain curves and flexural strength

Fig. 12 shows the stress-strain curves for bending behaviour at different infill densities and specimen types with honeycomb-shaped infill patterns. The stress-strain curves exhibit variations that correspond to both the infill density and the honeycomb infill pattern of

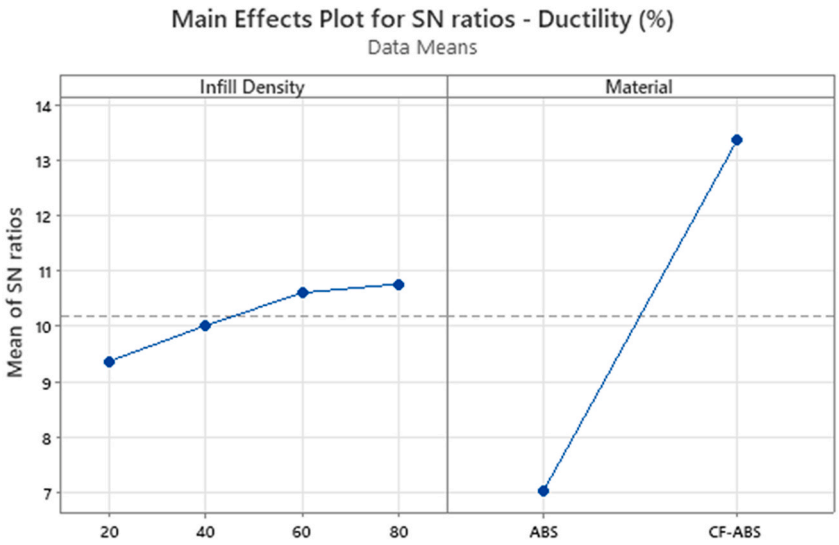

Fig. 9. Main effects plot for ductility Vs infill density for ABS and CF-ABS materials.

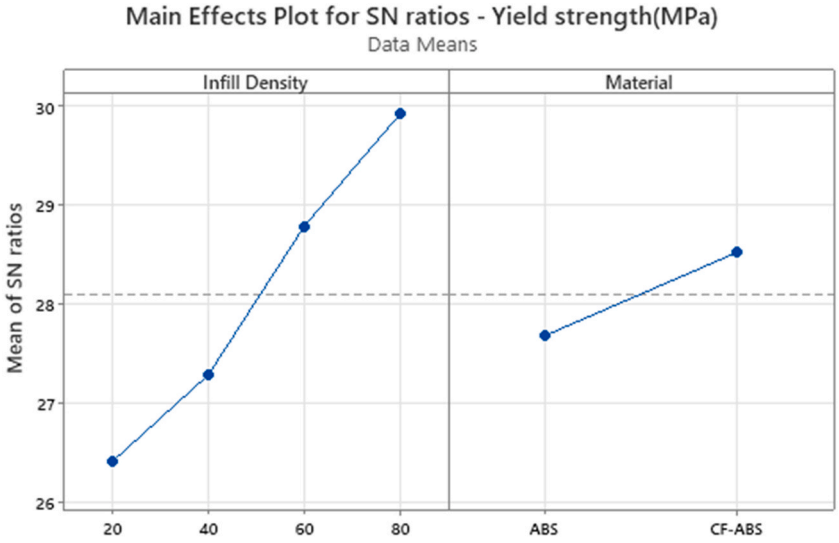

Fig. 10. Main effects plot for yield strength Vs infill density for ABS and CF-ABS materials.

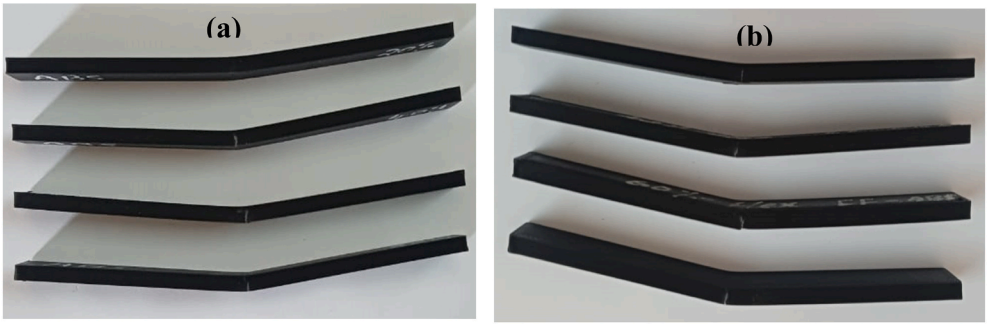

Fig. 11. Fracture behaviour of specimens after compressive test response (a) ABS and (b) CF-ABS.

Table 4
Results of L_8 array of the Taguchi mixed level design of experiment for flexural test

Run	Output parameter		
	Flexural Strength (MPa)	Flexural modulus (GPa)	Flexural Strain (%)
1	59.423 ± 2.24	1.296 ± 0.04	1.032 ± 1.01
2	64.837 ± 3.62	1.437 ± 0.91	1.671 ± 0.33
3	71.254 ± 4.66	1.688 ± 0.04	2.942 ± 0.44
4	76.687 ± 5.91	2.381 ± 0.14	3.812 ± 0.51
5	71.132 ± 1.23	5.276 ± 0.78	2.041 ± 0.61
6	83.746 ± 1.84	5.454 ± 0.88	3.713 ± 0.81
7	105.911 ± 2.45	6.278 ± 0.17	4.135 ± 0.54
8	128.423 ± 3.56	7.361 ± 0.48	4.691 ± 0.67

ABS and CF-ABS, as shown in Fig. 12(a) and 8(b). Fig. 12(a) and 8(b) demonstrate an increasing trend in the stress-strain curves as the infill density increases. At 80 % infill density, the stress-strain curve of CF-ABS with a honeycomb-type infill pattern displayed a higher maximum value than that of ABS. However, ABS and CF-ABS filament-type material were found to be the lowest in specimens with a honeycomb-type infill pattern and 20 % infill density.

Following the findings shown in Fig. 12(a), the flexural strength of ABS with a honeycomb-type infill pattern at 20 % infill density was significantly lower at 59.423 MPa compared to the 80 % infill density, which had a higher flexural strength of 76.687 MPa. The stress-strain curve for the ABS's flexural behaviour showed a sudden decrease in stress value and breakage, accompanied by average

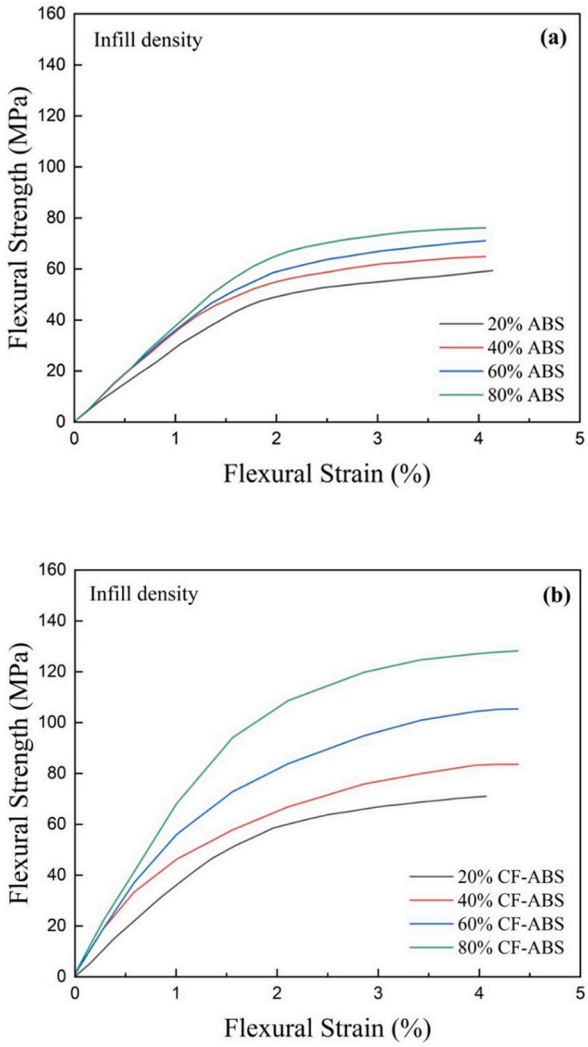

Fig. 12. F Flexural stress-strain curves for various honeycomb-type infill patterns (a) ABS and (b) CF-ABS.

standard deviation values. These findings suggest that the test results may fluctuate due to inadequate interface bonding that occurs among the layers of the specimen. The results shown in Fig. 12(b) show that the CF-ABS material had the highest UTS of 128.423 MPa when it was filled with a honeycomb-shaped pattern and a density of 80 %. This result surpassed that of the ABS material, which demonstrated a UTS of 76.687. Additionally, the CF-ABS material's flexural stress increased by 67.46 %. At the midpoint, we observed bending delamination in the CF-ABS specimens rather than an abrupt fracture towards the periphery of the applied load [27,29].

3.2.2. Flexural modulus

Fig. 13 shows the flexural modulus of the ABS and the CF-ABS samples with various infill densities and honeycomb-type infill pattern types. From Fig. 13(a), it is evident that the 20 % infill density of ABS with the honeycomb-type infill pattern shows the lowest flexural modulus of 1.294 GPa, in contrast to the 80 % infill density of 2.381 GPa. Poor-quality 3D-printed ABS specimens with lower flexural stress and decreasing fiber content in the matrix yielded the lowest modulus values. Fig. 13(b) reveals that CF-ABS, with an 80 % infill density and a honeycomb type infill pattern, achieved the highest flexural modulus of 7.361 GPa, surpassing Re-PLA's 2.381 GPa by 209.15 % in both modulus and strain increases, respectively. However, increasing the fibre reinforcement concentration within the matrix material increases the flexural modulus [28].

3.2.3. Main effects plot for flexural test

The main effects plots for flexural strength as well as the flexural modulus are as shown in Figs. 14 and 15, which demonstrates the substantial impact of specific factors on the observed response. However, the flexural strength and flexural modulus are influenced by

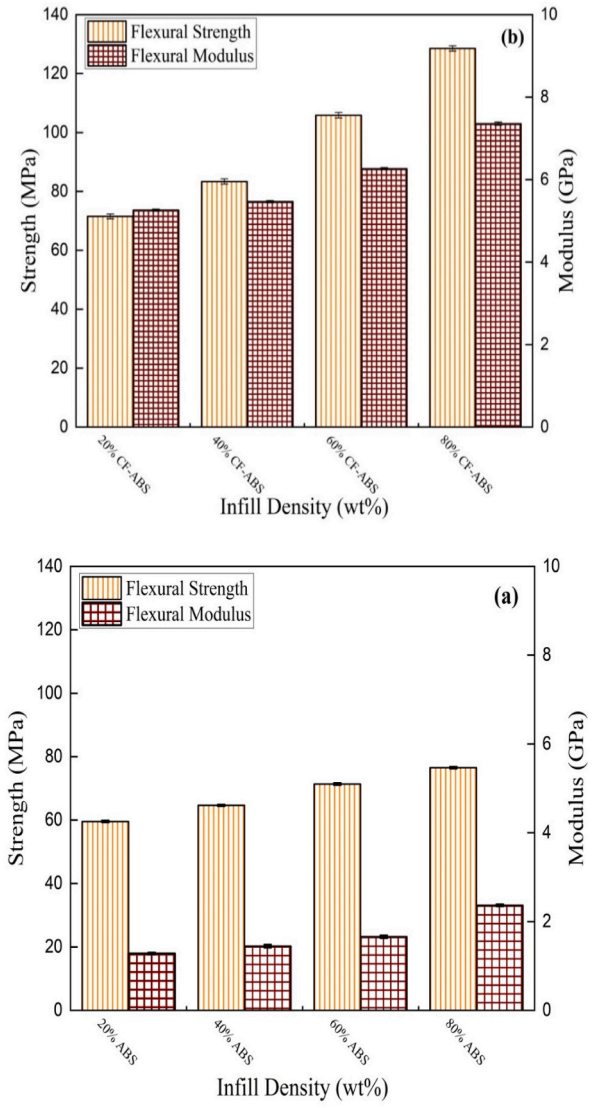

Fig. 13. Flexural strength Vs flexural modulus for varying infill density along with honeycomb type infill pattern (a) ABS and (b) CF-ABS.

the 20 % infill density of ABS filament material out of the other infill process parameters. The highest flexural strength (64.74 %) and flexural modulus (209.15 %) were observed at the maximum infill density at 240 °C nozzle temperature and 45 mm/min print speed for honeycomb filled pattern. At lower print speeds and infill densities, the flexural strength of the specimen is significantly diminished due to the presence of pores along with the gaps amidst each produced raster angle [46,53].

3.3. Compressive test response of ABS and CF-ABS

The compressive test was conducted to do a comparison among compressive properties of 3D printed samples for every group of infill density and honeycomb-type pattern specimens. Fig. 16 illustrates the fractured specimens following the completion of the compressive test. Fig. 16 (a) depicts the fracture behaviour of specimens after compressive test response for ABS, while Fig. 16 (b) depicts the fracture behaviour of specimens after compressive test response for CF-ABS. As per ASTM D695, the validity of a compressive test is contingent upon the occurrence of shear fractures at the applied compressive load, as well as the observation that the maximum strain at the outermost part of the sample breakdown falls inside the prescribed 30 % strain limit. In the present investigation, it was observed that none of the specimens experienced fracture beyond the imposed strain threshold of 30 %. The experimentally obtained values of compressive strength as well as compressive modulus are presented in Table 5. Incorporating CFs significantly enhances compressive strength in composites compared to pure ABS counterparts, regardless of infill densities, indicating improved load-bearing capacity and resistance to compression. CF-ABS composites consistently display increased strength with higher infill densities, while variability exists in pure ABS composites due to factors like interlayer adhesion and voids. Notably, at 80 % infill, CF-ABS surpasses pure ABS by 66.821 MPa–55.117 MPa, illustrating the synergistic effect of CF reinforcement and higher infill densities. Similarly, CFs inclusion leads to a substantial increase in yield strength compared to pure ABS composites across varying infill densities, indicating improved deformation resistance and overall material strength [33]. While CF-ABS composites consistently exhibit increased yield strength with higher infill densities, variability exists in pure ABS composites due to factors like interlayer adhesion and voids. At 80 % infill, CF-ABS yields 58.01 GPa, significantly higher than pure ABS at 49.43 GPa, highlighting the synergistic effect of CF reinforcement and increased infill densities on mechanical properties. Furthermore, CFs inclusion notably enhances compressive modulus compared to pure ABS composites, regardless of infill densities, indicating increased rigidity and stiffness due to CF reinforcement [46]. While CF-ABS composites consistently display increased modulus with higher infill densities, variability exists in pure ABS composites due to factors like interlayer adhesion and voids [41]. At 80 % infill, CF-ABS exhibits a compressive modulus of 2.273 GPa, significantly higher than pure ABS at 1.473 GPa, emphasizing the synergistic effect of CF reinforcement and increased infill densities on mechanical characteristics.

3.3.1. Compressive stress-strain curves

Fig. 17(a) and (b) exhibit the specimens' compressive stress-strain curves within every group, representing a typical trend. As demonstrated in Fig. 17(a) and 18(b), both during compression tests, stress-strain curves increase with increasing infill density. The CF-ABS, with an 80 % infill density and a grid-type infill pattern, had the best stress-strain curve compared to ABS. The lowest stress-strain curves were seen for both ABS and CF-ABS filament-type materials when specimens had 20 % infill density and a honeycomb-type infill pattern.

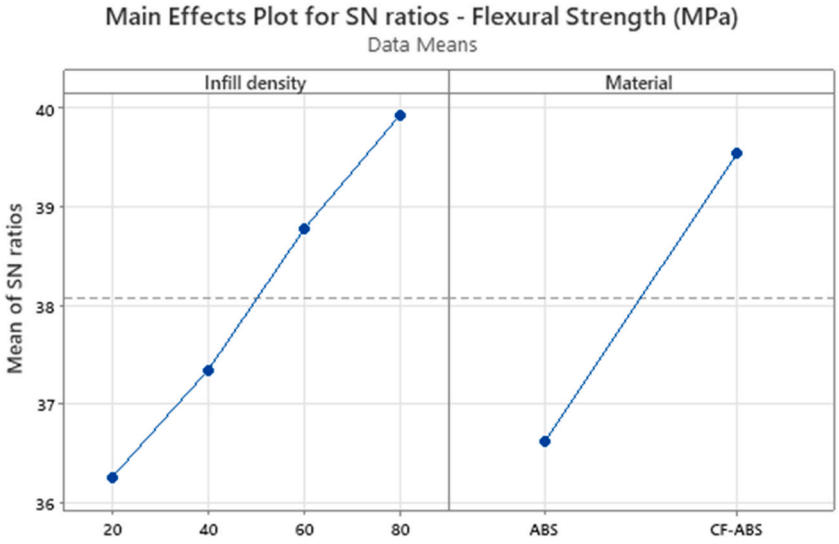

Fig. 14. Main effects plot for flexural strength Vs infill density for ABS and CF-ABS materials.

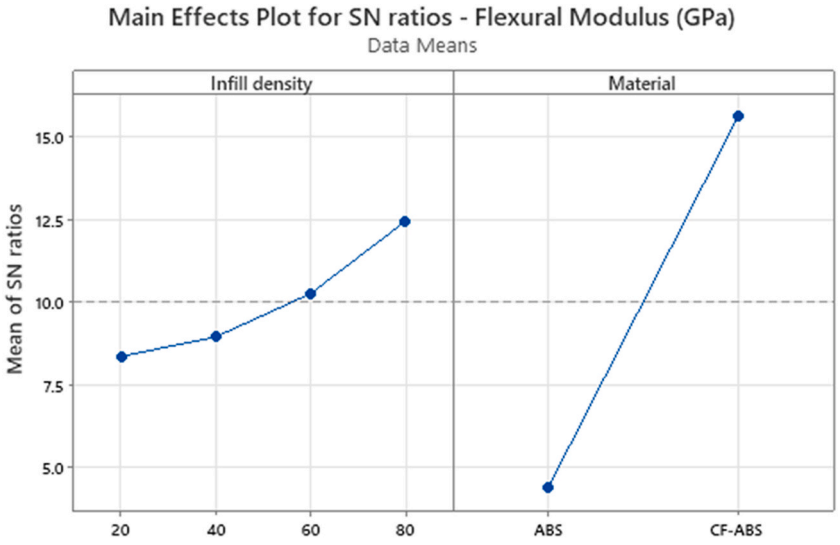

Fig. 15. Main effects plot for flexural modulus Vs infill density for ABS and CF-ABS materials.

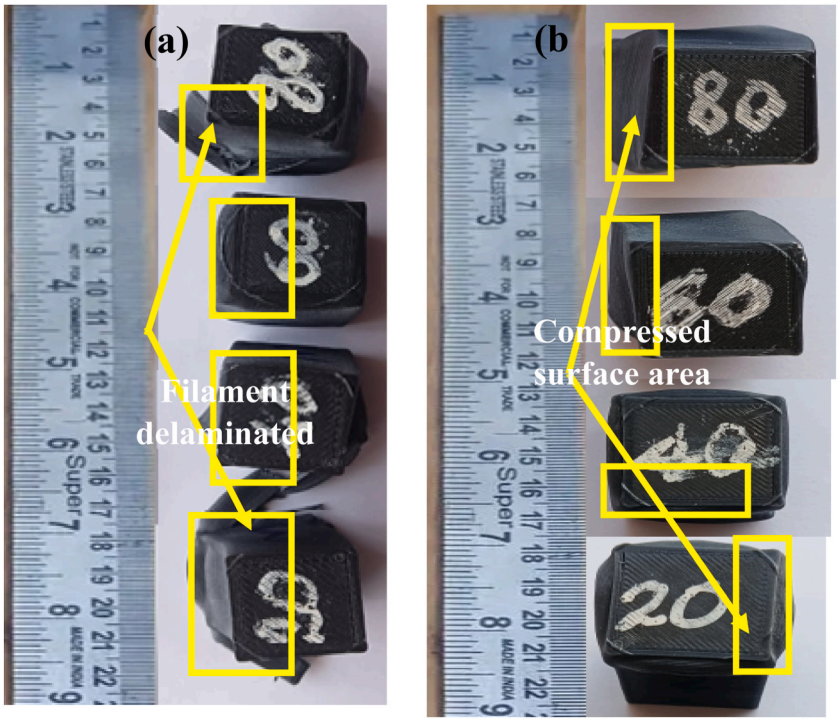

Fig. 16. Fracture behaviour of specimens after compressive test response (a) ABS and (b) CF-ABS.

3.3.2. Compressive strength

In Fig. 17, the compressive strengths of ABS and CF-ABS samples with various infill densities and honeycomb-type infill patterns are shown. The graph (Fig. 17(a)) shows that the 20 % infill density of ABS with the honeycomb-type infill pattern had the lowest compressive strength, at 29.671 MPa. The 80 % infill density had the highest strength, at 56.312 MPa. During compression testing, pressure aligns the specimen in relation to its height, causing adjacent layers to experience shear stress due to additive buildup. Layers sliding against one another create a shear force that can easily break specimens. Fig. 17(b) demonstrates that CF-ABS, with an 80 % infill density and a honeycomb-type infill pattern, achieves the highest ultimate compressive strength of 66.821 MPa, surpassing ABS's 29.671 MPa, resulting in a 125.21 % increase in compressive strength. This is because fewer cracks form at the center of the specimens due to reduced gaps, which radiate outward and increase plastic deformation resistance. Thus, CF-ABS specimens with a honeycomb

Table 5
Results of L_8 array of the Taguchi mixed level design of experiment for compressive test

Run	Output parameter			
	Compressive Strength (MPa)	Yield Strength (GPa)	Compressive modulus (GPa)	Compressive Strain (%)
1	29.671 ± 1.656	23.41 ± 1.12	0.624 ± 0.01	2.209 ± 1.052
2	43.567 ± 2.882	27.32 ± 2.24	0.828 ± 0.02	2.393 ± 0.487
3	51.232 ± 3.639	37.23 ± 2.18	0.850 ± 0.09	3.292 ± 1.063
4	56.312 ± 5.572	39.12 ± 1.98	1.091 ± 0.99	3.429 ± 1.451
5	35.103 ± 2.102	25.02 ± 1.47	0.838 ± 0.03	2.271 ± 0.511
6	47.615 ± 2.863	36.42 ± 2.08	0.901 ± 0.09	3.916 ± 1.063
7	55.117 ± 3.184	49.43 ± 1.01	1.473 ± 0.85	5.154 ± 1.121
8	66.821 ± 4.112	58.01 ± 1.92	2.273 ± 0.92	5.914 ± 1.142

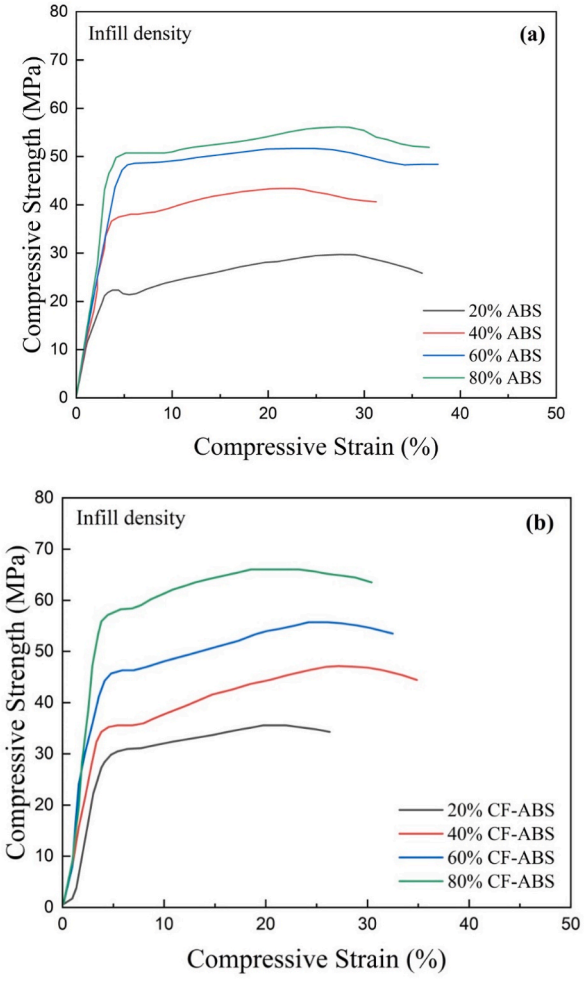

Fig. 17. Compressive stress-strain curves for varying infill density along with honeycomb-type infill pattern (a) ABS and (b) CF-ABS.

pattern achieve the highest compression strength compared to ABS, PLA, and CF-PLA materials [31,46]. Moreover, considering the impact of lower infill density and triangular infill patterns, PLA exhibits lower compressive strength than PLA-CF [54], and ABS [51] while ABS demonstrates higher compressive strength than PLA [46,54] and PLA-CF, particularly under higher infill density, rectilinear/grid type patterns, and elevated temperatures or dynamic loading conditions [55].

3.3.3. Compressive modulus

Fig. 18 shows the compressive modulus of the ABS and CF-ABS 3D-printed samples with various infill densities and honeycomb-type infill pattern types. Fig. 18(a) concludes that the 20 % infill density of ABS with the honeycomb-type infill pattern exhibited the lowest compressive modulus of 0.624 GPa, compared to the 80 % infill density of 1.091 GPa. As a result, the ABS with honeycomb-type

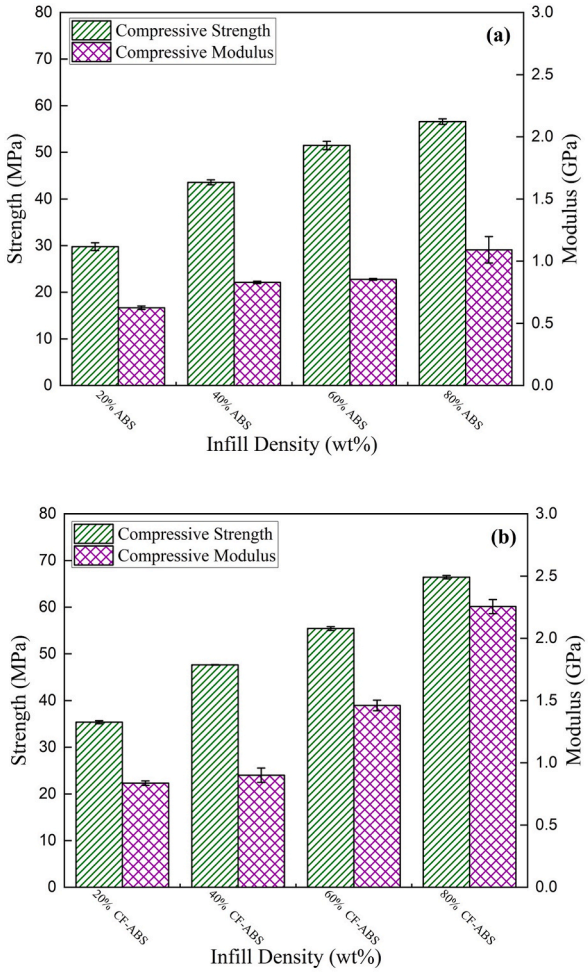

Fig. 18. Compressive strength with respect to compressive modulus for varying infill density along with honeycomb type infill pattern (a) ABS and (b) CF-ABS.

fill pattern specimen's yield strength increases with the increase in infill density and compressive modulus and is plastically deformed compared to other infill densities. Fig. 18(b) reveals that CF-ABS with a honeycomb infill pattern at 80 % infill density achieved the highest compressive modulus of 2.273 GPa, surpassing ABS with 1.091 GPa by 108.34 %, yield strength by 48.78 %, and strain by 72.47 %, respectively. However, the Fig. 18(b) shows that the addition of CF filament improves the smallest yield strengths for all 3D printed CF-ABS specimens, resulting in the highest compressive modulus [52].

3.3.4. Main effects plots for compressive test

The main effects plot for compressive strength and compressive modulus versus infill density and ABS/CF-ABS are as shown in Figs. 19 and 20 that demonstrate the response and significance of each parameter. However, the compressive strength and compressive modulus are meagrely influenced by the lower infill density in addition to the other parameters. The highest compressive strength and compressive modulus were achieved with honeycomb infill pattern at 80 % infill density. Changing the infill density doesn't have much of an effect on the compressive properties of the three patterns—triangular, grid, and trihexagonal [54]. This is because the patterns' size and shape determine the compressive properties [55,52].

3.4. Izod impact testing

The 3D printed ABS as well as the CF-ABS samples with different infill densities and honeycomb samples of infill patterns have been made in accordance with the ASTM D256 standard to investigate their energy absorption capacity employing the Izod impact test. Fig. 21 depicts the experimental configuration employed for impact characterization. To assess the energy absorption capacity of each sample, the pendulum mass, swing length, and impact speed employed were 2.0 kg, 390 mm, and 3.85 m s^{-1}, respectively. Five specimens, each measuring 80 mm × 12.7 mm × 3 mm, were utilized to assess the impact strength.

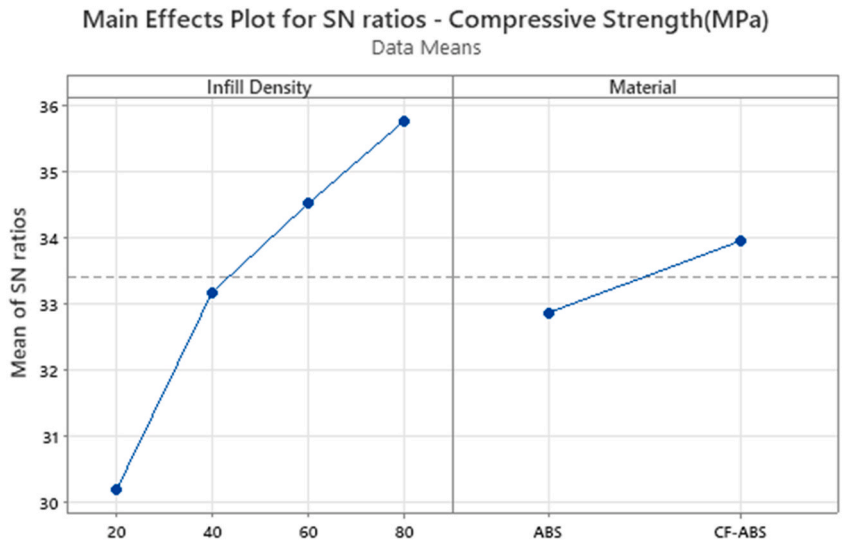

Fig. 19. Main effects plot for compressive strength Vs infill density for ABS and CF-ABS materials.

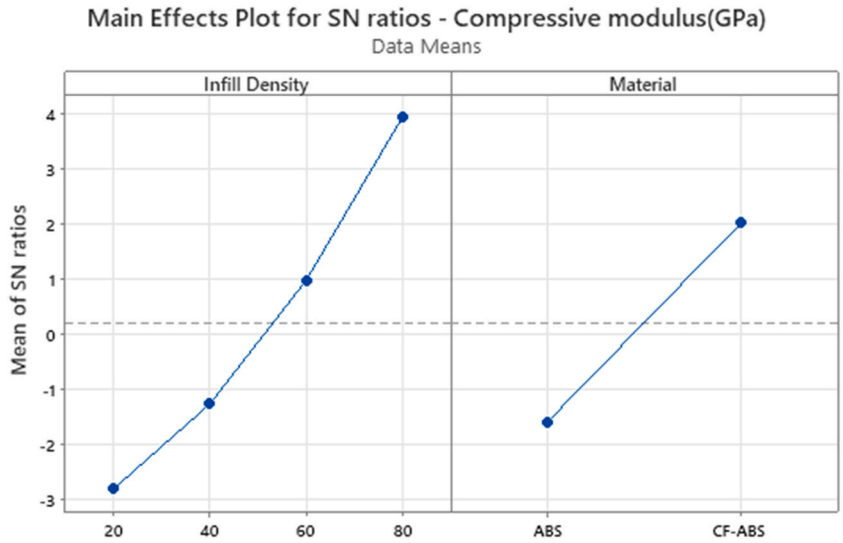

Fig. 20. Main effects plot for compressive modulus Vs infill density for ABS and CF-ABS materials.

3.4.1. Izod impact strength

Fig. 22 shows the results of average energy absorption capacity of ABS and CF-ABS specimens derived from Izod impact test. With an increase of infill density in ABS and CF-ABS samples the energy absorption capacity also increases. Further, Fig. 22 reveals that the insertion of individual infill density with honeycomb filled pattern by 0.2 wt% in CF-ABS is increased by 38.91 % (166.421 ± 2.61 J) as compared to ABS (119.811 ± 1.226 J). The inclusion of various infill densities in CF-ABS also exhibits similar behaviour which are 4.42, 10.64 and 12.11 % for 20, 40 and 60 wt%, respectively, as compared to ABS. The experimentally obtained values of Izod impact strengths are presented in Table 6. As an illustration, when the infill density is set at 80 %, the CF-ABS composite demonstrates a significantly greater impact strength of 166.421 J/m in comparison to the pure ABS composite with its impact strength of 145.207 J/m. The CF-ABS has an impact strength of 166.421 J/m, which is higher than the impact strengths (40 J/m and 113.12 J/m) found in the academic literature for pure PLA and CF-PLA samples [56–60]. This observation demonstrates the combined impact of CF reinforcing and increased infill densities on the improvement of toughness and impact resistance in composite materials. The enhanced impact strength observed in this study suggests that the incorporation of fibre reinforcement has a positive influence. This finding is consistent with the impact strength values reported in previous research (up to 150 J/m) for carbon fibre-reinforced polylactic acid [36]. Furthermore, it corroborates the existing literature findings on the mechanical characteristics of PLA composites. Specifically, Lou et al. [59] reported a value of 85.45 J/m for the impact strength of PLA composites with a 15 % fibre content. The inclusion of CFs in various infill densities leads to a substantial improvement in Izod impact strength as compared with pure ABS counterparts. This

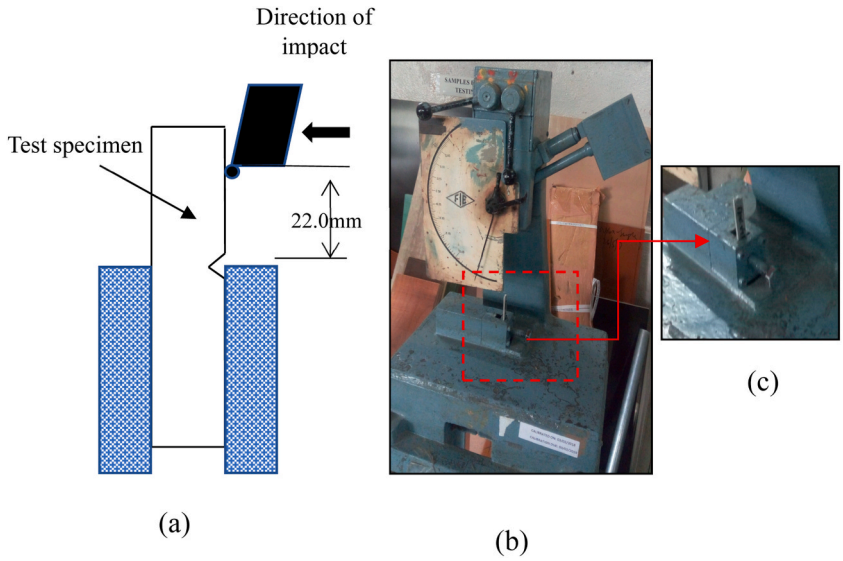

Fig. 21. Experimental setup (a) Impact test dimensions, (b) Izod impact test instrument and (c) Specimen position on the machine for the impact test.

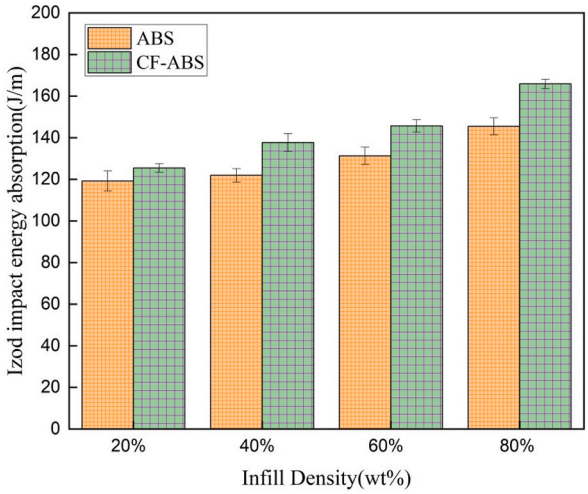

Fig. 22. Energy absorption of 3D printed ABS and CF-ABS specimens of 20, 40, 60 and 80 % infill densities under Izod impact test.

Table 6
Results of L_8 array of the Taguchi mixed level design of experiment for impact test

Run	Output parameter
	Izod impact Strength (J/m)
1	119.811 ± 1.226
2	122.547 ± 1.412
3	131.232 ± 2.019
4	146.312 ± 2.172
5	125.113 ± 1.321
6	137.415 ± 1.163
7	145.207 ± 2.114
8	166.421 ± 2.612

improvement signifies enhanced durability and resilience against impact because of CF reinforcement. Incorporating CFs into the ABS matrix enhances the material's strength, hence increasing its resistance to fracturing when subjected to impact stresses. In comparison to pure ABS composites, CF-ABS composites typically demonstrate superior impact strength at all infill densities. The observed variability can be ascribed to various factors, including interlayer adhesion, prevents crack propagation and the presence of voids within the printed component. These characteristics have the potential to influence the material's capacity to absorb and disperse energy when subjected to impact loading. The comparison of Izod impact strength values among various composite codes reveals a notable enhancement resulting from the use of CFs, particularly when larger infill densities are utilized.

3.4.2. Main effects plot for Izod impact test

The main effects plot for Izod impact strength is as shown in (Fig. 23), which demonstrates the substantial impact of individual infill density parameters versus the response of ABS as well as CF-ABS filament materials for honeycomb filled pattern. However, the impact strength is most impacted by the lower percentage infill density among the other higher percentage infill density, print speed along with the nozzle temperature process parameters. The highest impact strength (38.91 %) is obtained at the 80 % infill density with CF-ABS filament material for honeycomb filled pattern at constant nozzle temperature (240 °C) and print speed (45 mm/s). For trihexagonal pattern, triangular pattern and grid pattern, the impact property remains unchanged throughout the infill density range of 50–100 % [56,58] in comparison to honeycomb or hexagonal pattern [57,60].

3.5. SEM morphology of fractured CF-ABS composites

The results of the tensile, flexural and compressive tests demonstrate that CF-ABS displays higher strength characteristics when compared to ABS. SEM was used to study the morphology of the fracture interface in the samples, aiming to understand deformation and fracture mechanisms. A single specimen was chosen from each infill density category (20 %, 40 %, 60 % and 80 %) based on its ability to accurately represent the observed failure mode. The samples were examined in more detail, focusing on how the thermoplastic matrix of CF-ABS adhered to the samples using SEM morphology.

The cross-sectional views of the specimens from each infill density group (20 %, 40 %, 60 % and 80 %) after the tensile test are shown in Fig. 24(a)–(d). The results show that the CF-ABS sample with a 20 % infill density had fibres pulling out, matrix cracking, fibre breakage, and rupture at the interface, which means it didn't stick together. Fig. 24(a) depicts the detached layers from one another. In CF-ABS samples with infill densities of 40 %, 60 % and 80 % changes in the fracture surface topography can be seen, such as changes in surface roughness, fibre pull-out lengths, and fibre bridging effects. these specimens have CF fibres, their surfaces look uneven, and the crack becomes visible as each layer of the 3D print breaks apart after the test [33], as shown in Fig. 24(b)–(d).The fracture analysis can inform based on the material selection, process parameters, and post-processing techniques to enhance the reliability, durability and performance of printed parts [34].

Fig. 25(a)–(d) illustrate the results of compressive testing using CF-ABS 3D-printed materials. Each figure represents a different group of thermoplastic matrix composites with infill densities of 20 %, 40 %, 60 % and 80 %. The results in Fig. 25(a) indicate that during a compressive test of 20 % infill density, fracture elements such as delamination, fibre orientation, matrix deformation, fibre-matrix adhesion, micro-cracks and interfacial debonding were induced. The phenomena observed in Fig. 25 (b) suggest that the layers of the specimen separated and created voids between them due to the compressive pressure applied. The presence of CFs in CF-ABS under compression affects its fracture behaviour through mechanisms like fibre buckling, kinking, micro-buckling and matrix crushing

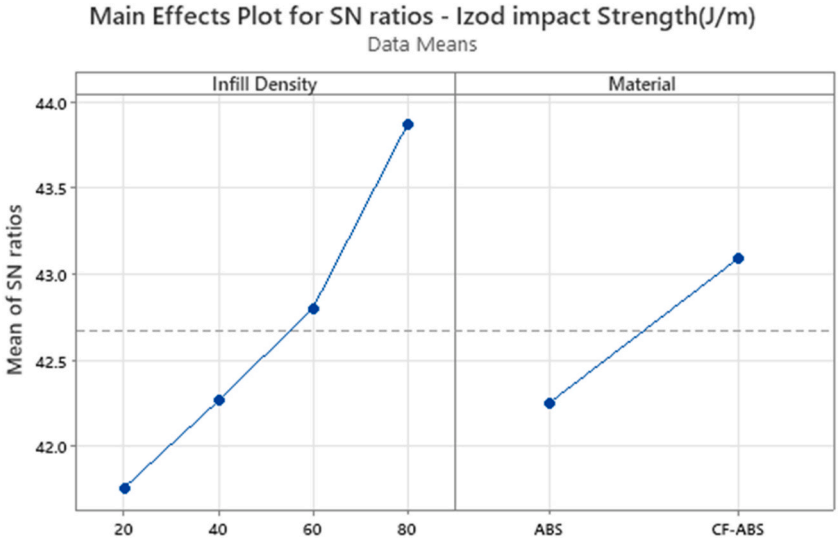

Fig. 23. Main effects plot Izod strength Vs infill density for ABS and CF-ABS materials.

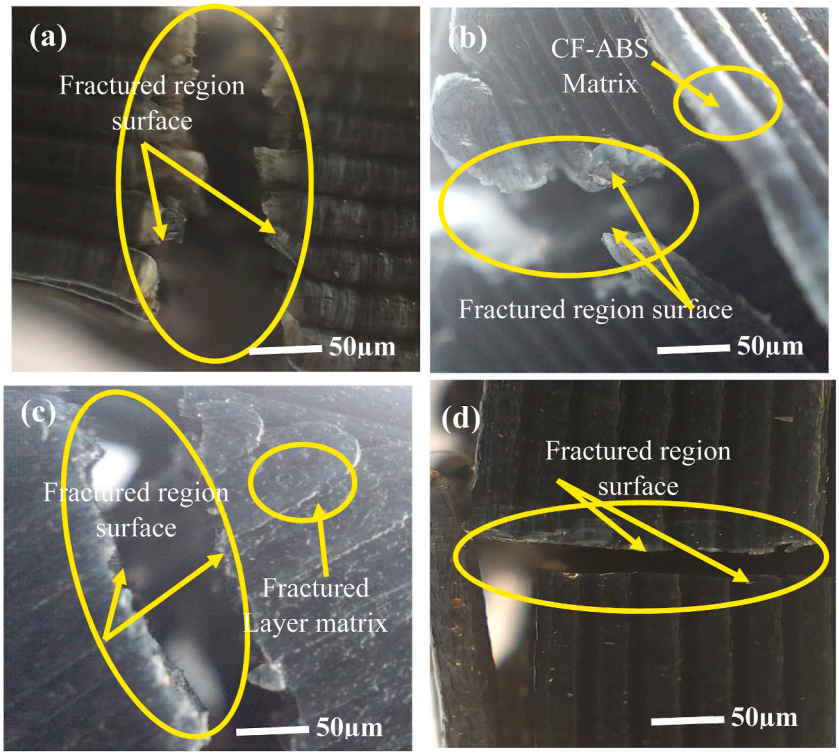

Fig. 24. Images from a SEM showing the cracked surface of CF-ABS composites at (a) 20 %, (b) 40 %, (c) 60 %, and (d) 80 % after a tensile test.

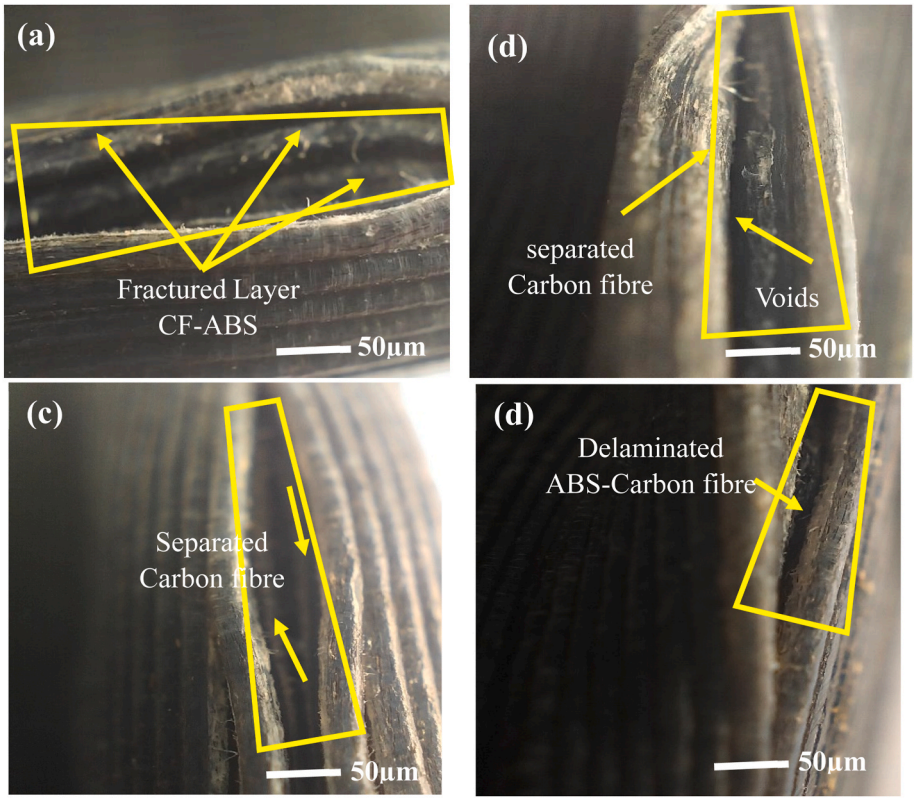

Fig. 25. SEM images of the CF-ABS composites' cracked surfaces after a compressive test at 20 %, 40 %, 60 %, and 80 %.

[12], as illustrated in Fig. 25(c). As shown in Fig. 25(d), the 80 % infill density type exhibits strong bonding between the printed layers and the matrix, indicating that they bond well with each other.

In Fig. 26(a)–(d), the specimens' cross-sectional profiles following flexural testing are visible. Fig. 26(a) illustrates the absence of interlayer adhesion in CF-ABS, as evidenced by the fibre-matrix interactions, voids and crack propagation paths and distinct fracture region. In addition, Fig. 26(b) demonstrates that CF-ABS has a non-uniform fracture pattern despite enhanced adhesion. In Fig. 26(c), the split CF-ABS matrix is clearly visible as fibre orientation, matrix cracking, fibre-matrix adhesion, delamination and any signs of fibre pull-out or fracture brought on by flexural loading. Finally, the CFs were joined within the matrix, indicating that the mechanical properties had improved by transferring the load from the CF-ABS to the CFs [33], as shown in Fig. 26(d).

4. Conclusion

The objective of the study was to determine the optimal infill density settings for enhancing the compressive, flexural, tensile, and Izod impact properties of ABS and CF-ABS 3D-printed composites. The assessment covered properties such as tensile strength, flexural strength, compressive strength and impact strength. The specific conclusions listed below can be drawn.

- The infill density with 80 % of CF-ABS filament material with a honeycomb pattern showed a higher tensile strength of 36.9222 MPa, Young's modulus of 1.932 Gpa and ductility of 33.621 Mpa than the ABS filament material. The honeycomb lattice structure enhances heat treatment efficacy in 3D printed CF-ABS parts, resulting in greater bonds and increased infill density due to increased tensile strength, Young's modulus and ductility.
- The flexural strength as well as the flexural modulus of CF-ABS were improved by 64.74 % and 209.15 %, respectively, compared to ABS material. Reinforcing material absorbs matrix material, reducing porosity and allowing greater load strength because of the enhanced interfaces, resulting in improved flexural mechanical properties.
- The compressive strength and compressive modulus of CF-ABS increased by 125.21 % and 108.34 % compared to ABS composites, reducing air gaps and physical properties, thereby increasing plastic deformation resistance.
- The Izod impact strength of CF-ABS increased by 38.91 % compared to ABS, influenced by infill density and print speed parameters, but raster-to-raster air gap persists.

Optimizing infill density enables manufacturers and researchers to customize 3D printed parts' mechanical properties, resulting in lightweight structures, functional prototypes, and components with specific load-bearing capabilities. The performance of these

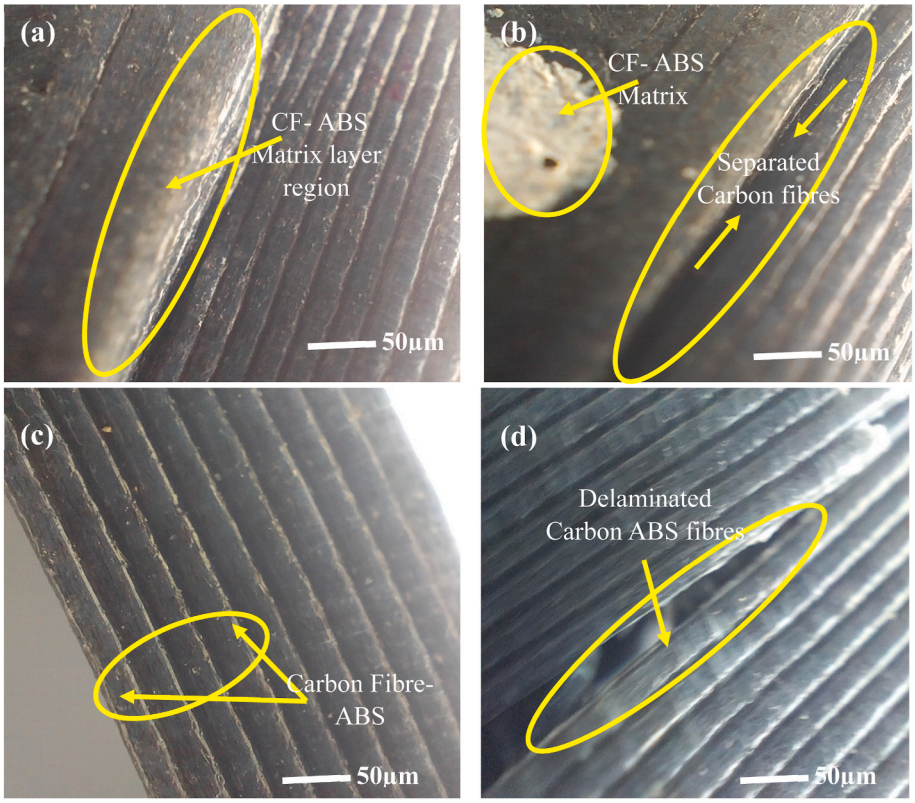

Fig. 26. SEM images of the CF-ABS composites' flexural test cracked surfaces at (20), (b), (c), (60) and (d) 80 %.

composites under different loading circumstances can be better understood by doing future study into their fatigue behaviour and long-term durability.

CRediT authorship contribution statement

Seshaiah Turaka: Writing – original draft, Resources, Methodology, Investigation, Formal analysis. **Venumurali Jagannati:** Validation, Resources, Investigation. **Bridjesh Pappula:** Resources, Project administration, Methodology. **Seshibe Makgato:** Writing – review & editing, Supervision.

Declaration of competing interest

The authors declare that they have no known competing financial interests or personal relationships that could have appeared to influence the work reported in this paper.

Nomenclature

σ_F	Flexural stress (N/mm^2)
σ_{F1}, σ_{F2}	Flexural stresses at the predefined points on the load-deflection curve
ϵ_{F1}, ϵ_{F2}	Flexural strain values at the predetermined point on the load deflection curve
$\Delta\sigma c$	The difference in applied compressive stress between two strain points
$\Delta\epsilon c$	The difference between applied compressive two strain points
$\Delta\sigma$	The difference in applied tensile stress between two strain points
$\Delta\epsilon$	The difference between the two strain points
b	The width of the specimen (mm)
d	The depth of the specimen (mm)
A	The average cross-sectional area (mm^2)
Ac	Minimum cross-sectional area (mm^2)
E	Young's modulus (GPa)
E_c	Compressive modulus (GPa)
E_F	Flexural modulus (GPa)
F_c	Maximum compressive strength (MPa)
F_{ut}	Ultimate Tensile Strength (MPa)
$P_{c\ max}$	Maximum compressive load before failure (N)
P_{max}	The maximum load before failure (N)
P	Load applied at a given mid-point on the specimen (N)
L	Length of the span (mm)
ABS	Acrylonitrile Butadiene Styrene
CF	Carbon Fibre
CF-ABS	Carbon Fibre Reinforced-Acrylonitrile Butadiene Styrene
CF-PEEK	Carbon Fibre- Polyether ether Ketone
FFF	Fused Filament Fabrication
GF-PEEK	Glass Fibre- Polyether Ether Ketone
MEX	Metal Extrusion
OA	Orthogonal Array
OM	Optical Microscopy
PET-G	Polyethylene Terephthalate Glycol
PLA	Poly Lactic Acid
SCRF-ABS	Short Carbon Fibre Reinforced- Acrylonitrile Butadiene Styrene
SEM	Scanning Electron Microscopy
TPU	Thermoplastic Polyurethane
UTM	Universal Testing Machine
UTS	Universal Tensile Strength (MPa)
UV	Ultraviolet

References

[1] M.T. Birosz, D. Ledenyak, M. Ando, Effect of FDM infill patterns on mechanical properties, Polym. Test. 113 (2022) 107654, https://doi.org/10.1016/j.polymertesting.2022.107654.
[2] F.M. Mwania, M. Maringa, J. Nsengimana, Investigating the effect of process parameters on the degree of fusion of two adjacent tracks produced through fused deposition modelling of acrylonitrile butadiene styrene, Polym. Test. 121 (2023) 107981, https://doi.org/10.1016/j.polymertesting.2023.10798.
[3] Ganesh Iyer S. Srinivasan, O. Keles, Effect of raster angle on mechanical properties of 3D printed short carbon fiber reinforced acrylonitrile butadiene styrene, Compos. Commun. 32 (2022) 101163, https://doi.org/10.1016/j.coco.2022.101163.
[4] A.K. Cress, J. Huynh, E.H. Anderson, R. O'neill, Y. Schneider, O. Keles, Effect of recycling on the mechanical behavior and structure of additively manufactured acrylonitrile butadiene styrene (ABS), J. Clean. Prod. 279 (2021) 123689, https://doi.org/10.1016/j.jclepro.2020.123689.
[5] J.D. Kechagias, S.P. Zaoutsos, An investigation of the effects of ironing parameters on the surface and compression properties of material extrusion components utilizing a hybrid-modeling experimental approach, Prog Addit Manuf (2023), https://doi.org/10.1007/s40964-023-00536-2.

[6] John Kechagias, Dimitrios Chaidas, Fused filament fabrication parameter adjustments for sustainable 3D printing, Mater. Manuf. Process. 38 (8) (2023) 933–940, https://doi.org/10.1080/10426914.2023.2176872.

[7] John Kechagias, Stephanos Zaoutsos, Effects of 3D-printing processing parameters on FFF parts' porosity: outlook and trends, Mater. Manuf. Process. 39 (6) (2024) 804–814, https://doi.org/10.1080/10426914.2024.2304843.

[8] John D. Kechagias, 3D printing parametric optimization using the power of Taguchi design: an expository paradigm, Mater. Manuf. Process. 39 (6) (2024) 797–803, https://doi.org/10.1080/10426914.2023.2290258.

[9] S. Doner, R. Paswan, S. Das, The influence of metallic particulate inclusions on the mechanical and thermal performance of 3D printable acrylonitrile-butadiene-styrene/thermoplastic polyurethane fused polymer blends, Mater. Today Commun. 35 (2023) 106111, https://doi.org/10.1016/j.mtcomm.2023.106111.

[10] J. Best, W. Freudenberg, N. Langhof, E. Schaffoner, Processing-microstructure correlations in material extrusion additive manufacturing of carbon fiber reinforced ceramic matrix composites, Addit. Manuf. 79 (2024) 103888, https://doi.org/10.1016/j.addma.2023.103888.

[11] A. Al Rashid, H. Ikram, M. Koç, Additive manufacturing and mechanical performance of carbon fiber reinforced Polyamide-6 composites, Mater Today Proc 62 (2022) 6359–6363, https://doi.org/10.1016/j.matpr.2022.03.339.

[12] P. Rezaeian, M.R. Ayatollahi, A. Nabavi-Kivi, N. Razavi, Effect of printing speed on tensile and fracture behavior of ABS specimens produced by fused deposition modeling, Eng. Fract. Mech. 266 (2022) 108393, https://doi.org/10.1016/j.engfracmech.2022.108393.

[13] A. Nabavi-Kivi, M.R. Ayatollahi, P. Rezaeian, N. Razavi, Investigating the effect of printing speed and mode mixity on the fracture behavior of FDM-ABS specimens, Theor Appl Fract 118 (2022) 103223, https://doi.org/10.1016/j.tafmec.2021.103223.

[14] S. Shahbaz, M.R. Ayatollahi, M. Petru, A.R. Torabi, U-notch fracture in additively manufactured ABS specimens under symmetric three-point bending, Theor Appl Fract. 119 (2022) 103318, https://doi.org/10.1016/j.tafmec.2022.103318.

[15] M.R. Khosravani, S. Rezaei, S. Faroughi, T. Reinicke, Experimental and numerical investigations of the fracture in 3D-printed open-hole plates, Theor Appl Fract 121 (2022) 103543, https://doi.org/10.1016/j.tafmec.2022.103543.

[16] K.M. Agarwal, P. Shubham, D. Bhatia, P. Sharma, H. Vaid, R. Vajpeyi, Analyzing the impact of print parameters on dimensional variation of ABS specimens printed using fused deposition modelling (FDM), Sens Int 3 (2022) 100149, https://doi.org/10.1016/j.sintl.2021.100149.

[17] P.M. Angelopoulos, G. Kenanakis, Z. Viskadourakis, P. Tsakiridis, K.C. Vasilopoulos, M.A. Karakassides, M. Taxiarchou, Manufacturing of ABS/expanded perlite filament for 3D printing of lightweight components through fused deposition modeling, Mater Today Proc 54 (2022) 14–21, https://doi.org/10.1016/j.matpr.2021.06.351.

[18] J. Brackett, D. Cauthen, J. Condon, T. Smith, N. Gallego, V. Kunc, C. Duty, The impact of infill percentage and layer height in small-scale material extrusion on porosity and tensile properties, Addit. Manuf. 58 (2022) 103063, https://doi.org/10.1016/j.addma.2022.103063.

[19] Abeykoon C, Sri-Amphorn P, Fernando A. Optimization of fused deposition modeling parameters for improved PLA and ABS 3D printed structures. Int J Lightweight Mater Manuf 202; 3: 284-297. https://doi.org/10.1016/j.ijlmm.2020.03.003.

[20] S. Cicero, M. Sánchez, V. Martínez-Mata, S. Arrieta, B. Arroyo, Structural integrity assessment of additively manufactured ABS, PLA and graphene reinforced PLA notched specimens combining Failure Assessment Diagrams and the Theory of Critical Distances, Theor Appl Fract 121 (2022) 103535, https://doi.org/10.1016/j.tafmec.2022.103535.

[21] A. Grant, B. Regez, S. Kocak, J.D. Huber, A. Mooers, Anisotropic properties of 3-D printed poly lactic acid (PLA) and acrylonitrile butadiene styrene (ABS) plastics, Results Mater 12 (2021) 100227, https://doi.org/10.1016/j.rinma.2021.100227.

[22] K.A. Al-Ghamdi, Sustainable FDM additive manufacturing of ABS components with emphasis on energy minimized and time efficient lightweight construction, Int J Lightweight Mater Manuf 2 (2019) 338–345, https://doi.org/10.1016/j.ijlmm.2019.05.004.

[23] F. He, Y.L.A. Alshammari, M. Khan, The effect of printing parameters on crack growth rate of FDM ABS cantilever beam under thermo-mechanical loads, Procedia Struct. Integr. 34 (2021) 59–64, https://doi.org/10.1016/j.prostr.2021.12.009.

[24] S. Garzon-Hernandez, D. Garcia-Gonzalez, A. Jérusalem, A. Arias, Design of FDM 3D printed polymers: an experimental-modelling methodology for the prediction of mechanical properties, Mater. Des. 188 (2020) 108414, https://doi.org/10.1016/j.matdes.2019.108414.

[25] M.S. Andrés, R. Chércoles, E. Navarro, J.M. de la Roja, J. Gorostiza, M. Higueras, E. Blanch, Use of 3D printing PLA and ABS materials for fine art. Analysis of composition and long-term behaviour of raw filament and printed parts, J. Cult. Herit. 59 (2023) 181–189, https://doi.org/10.1016/j.culher.2022.12.005.

[26] A.S. De León, A. Domínguez-Calvo, S.I. Molina, Materials with enhanced adhesive properties based on acrylonitrile-butadiene-styrene (ABS)/thermoplastic polyurethane (TPU) blends for fused filament fabrication (FFF), Mater. Des. 182 (2019) 108044, https://doi.org/10.1016/j.matdes.2019.108044.

[27] N. Yu, X. Sun, Z. Wang, Li J. Zhang, Effects of auxiliary heat on warpage and mechanical properties in carbon fiber/ABS composite manufactured by fused deposition modeling, Mater. Des. 195 (2020) 108978, https://doi.org/10.1016/j.matdes.2020.108978.

[28] Md Hazrat Ali, Syuhei Kurokawa, Essam Shehab, Mukhtarkhanov Muslim, Development of a large-scale multi-extrusion FDM printer, and its challenges, Int J Lightweight Mater Manuf 6 (2023) 198–213, https://doi.org/10.1016/j.ijlmm.2022.10.001.

[29] C.A. Suarez-Afanador, R. Cornaggia, N. Lahellec, A. Maurel-Pantel, D. Boussaa, H. Moulinec, S.P.A. Bordas, Effective thermo-viscoelastic behavior of short fiber reinforced thermo-rheologically simple polymers: an application to high temperature fiber reinforced additive manufacturing, Eur J Mech A Solids 96 (2022) 104701, https://doi.org/10.1016/j.euromechsol.2022.10470.

[30] P. Wang, B. Zou, S. Ding, L. Li, C. Huang, Effects of FDM-3D printing parameters on mechanical properties and microstructure of CF/PEEK and GF/PEEK, Chinese J Aeronaut 34 (2021) 236–246, https://doi.org/10.1016/j.cja.2020.05.040.

[31] J. Kluczyński, I. Szachogłuchowicz, J. Torzewski, L. Śnieżek, K. Grzelak, G. Budzik, Ł. Przeszłowski, M. Małek, J. Łuszczek, Fatigue and fracture of additively manufactured polyethylene terephthalate glycol and acrylonitrile butadiene styrene polymers, Int J Fatigue 165 (2022) 107212, https://doi.org/10.1016/j.ijfatigue.2022.107212.

[32] Z. Ali, Y. Yan, H. Mei, L. Cheng, L. Zhang, Effect of infill density, build direction and heat treatment on the tensile mechanical properties of 3D-printed carbon-fiber nylon composites, Compos. Struct. 304 (2023) 116370, https://doi.org/10.1016/j.compstruct.2022.116370.

[33] A. Forés-Garriga, G. Gómez-Gras, M.A. Pérez, Mechanical performance of additively manufactured lightweight cellular solids: influence of cell pattern and relative density on the printing time and compression behavior, Mater. Des. 215 (2022) 110474, https://doi.org/10.1016/j.matdes.2022.110474.

[34] W. Förster, T. Pucklitzsch, D. Dietrich, D. Nickel, Mechanical performance of hexagonal close-packed hollow sphere infill structures with shared walls under compression load, Addit. Manuf. 59 (2022) 103135, https://doi.org/10.1016/j.addma.2022.103135.

[35] I. Buj-Corral, A. Bagheri, A. Domínguez-Fernández, R. Casado-López, Influence of infill and nozzle diameter on porosity of FDM printed parts with rectilinear Hexagon pattern, Procedia Manuf. 41 (2019) 288–295.

[36] P. Bezaeian, M.R. Ayatollahi, A. Nabavi-Kivi, N. Razavi, Effect of printing speed on tensile and fracture behavior of ABS specimens produced by fused deposition modeling, Eng. Fract. Mech. 266 (2022) 108393, https://doi.org/10.1016/j.engfracmech.2022.108393.

[37] S.L. Rodríguez-Reyna, J.H. Díaz-Aguilera, H.R. Acevedo-Parra, C.J. García, E.J. Gutierrez-Castañeda, F. Tapia, Design and optimization methodology for different 3D processed materials (PLA, ABS and carbon fiber reinforced nylon PA12) subjected to static and dynamic loads, J. Mech. Behav. Biomed. Mater. 150 (2024) 106257, https://doi.org/10.1016/j.jmbbm.2023.106257.

[38] R.C. Daniel, P.E. Sudhagar, Vibration analysis of bio-inspired sandwich composite beam under rotating environment based on the Internet of Things technology, Mech. Base. Des. Struct. Mach. (2024), https://doi.org/10.1080/15397734.2024.2323151.

[39] V. Karupaiah, V. Narayanan, Influence of process parameters on ageing and free vibration characteristics of fiber-reinforced polymer composites by fusion filament fabrication process, Int. J. Mater. Res. 114 (10–11) (2023) 824–831, https://doi.org/10.1515/ijmr-2022-0271.

[40] N. Vidakis, M. Petousis, E. Velidakis, M. Liebscher, V. Mechtcherine, L. Tzounis, On the strain rate sensitivity of fused filament fabrication (Fff) processed pla, abs, petg, pa6, and pp thermoplastic polymers, Polymers 12 (12) (2020) 2924, https://doi.org/10.3390/polym12122924.

[41] M. Petousis, N. Vidakis, N. Mountakis, E. Karapidakis, A. Moutsopoulou, Compressive response versus power consumption of acrylonitrile butadiene styrene in material extrusion additive manufacturing: the impact of seven critical control parameters, Int. J. Adv. Des. Manuf. Technol. 126 (3) (2023) 1233–1245, https://doi.org/10.1007/s00170-023-11202-w.

[42] N. Vidakis, C. David, M. Petousis, D. Sagris, N. Mountakis, Optimization of key quality indicators in material extrusion 3D printing of acrylonitrile butadiene styrene: the impact of critical process control parameters on the surface roughness, dimensional accuracy, and porosity, Mater. Today Commun. 34 (2023) 105171, https://doi.org/10.1016/j.mtcomm.2022.105171.
[43] N. Vidakis, M. Petousis, A. Maniadi, E. Koudoumas, A. Vairis, J. Kechagias, Sustainable additive manufacturing: mechanical response of acrylonitrile-butadiene-styrene over multiple recycling processes, Sustainability 12 (9) (2020) 3568, https://doi.org/10.3390/su12093568.
[44] R.C. Parpala, D. Popescu, C. Pupaza, Infill parameters influence over the natural frequencies of ABS specimens obtained by extrusion-based 3D printing, Rapid Prototyp. J. 27 (6) (2021) 1273–1285, https://doi.org/10.1108/RPJ-05-2020-0110.
[45] C. Dudescu, L. Racz, Effects of raster orientation, infill rate and infill pattern on the mechanical properties of 3D printed materials, Acta Universitatis Cibiniensis. Technical Series 69 (1) (2017) 23–30, https://doi.org/10.1515/aucts-2017-0004.
[46] T.D. Do, M.C. Le, T.A. Nguyen, T.H. Le, Effect of infill density and printing patterns on compressive strength of ABS, PLA, PLA-CF materials for FDM 3D printing, InMaterials Science Forum 1068 (2022) 19–27, https://doi.org/10.4028/p-zhm1ra.
[47] ASTM D638-14: Standard Test Method for Tensile Properties of Plastics.
[48] ASTM D790-17: Standard Test Methods for Flexural Properties of Unreinforced and Reinforced Plastics and Electrical Insulating Materials.
[49] ASTM D695-23: Standard Test Method for Compressive Properties of Rigid Plastics.
[50] ASTM D256-23e1: Standard Test Methods for Determining the Izod Pendulum Impact Resistance of Plastics.
[51] M.R. Wisnom, The relationship between tensile and flexural strength of unidirectional composites, J. Compos. Mater. 26 (1992) 1173–1180, https://doi.org/10.1177/002199839202600805.
[52] M. Araya-Calvo, I. López-Gómez, N. Chamberlain-Simon, J.L. León-Salazar, T. Guillén-Girón, J.S. Corrales-Cordero, O. Sánchez-Brenes, Evaluation of compressive and flexural properties of continuous fiber fabrication additive manufacturing technology, Addit. Manuf. 22 (2018) 157–164, https://doi.org/10.1016/j.addma.2018.05.007.
[53] F. Ning, W. Cong, J. Qiu, J. Wei, S. Wang, Additive manufacturing of carbon fiber reinforced thermoplastic composites using fused deposition modeling, Compos. Part B Eng. 80 (2015) 369–378, https://doi.org/10.1016/j.compositesb.2015.06.013.
[54] M. Heidari-Rarani, M. Rafiee-Afarani, A.M. Zahedi, Mechanical characterization of FDM 3D printing of continuous carbon fiber reinforced PLA composites, Compos. Part B Eng. 175 (2019) 107147, https://doi.org/10.1016/j.compositesb.2019.107147.
[55] Z. Eren, C.A. Burnett, D. Wright, Z. Kazancı, Compressive characterization of 3D printed composite materials using continuous fibre fabrication, Int j lightweight mater manuf 6 (2023) 494–507, https://doi.org/10.1016/j.ijlmm.2023.05.002.
[56] A.A. Ansari, M. Kamil, Izod impact and hardness properties of 3D printed lightweight CF reinforced PLA composites using design of experiment, Int j lightweight mater manuf 5 (2022) 369–383, https://doi.org/10.1016/j.ijlmm.2022.04.006.
[57] L. Wang, W.M. Gramlich, D.J. Gardner, Improving the impact strength of poly (lactic acid) (PLA) in fused layer modeling (FLM), Polym 114 (2017) 242–248, https://doi.org/10.1016/j.polymer.2017.03.011.
[58] L.G. Blok, M.L. Longana, H. Yu, B.K.S. Woods, An investigation into 3D printing of fibre reinforced thermoplastic composites, Addit. Manuf. 22 (2018) 176–186, https://doi.org/10.1016/j.addma.2018.04.039.
[59] C. Lou, J. Liao, Z. Lin, J. Lin, Manufacturing and mechanical property evaluations of CF/PLA biocomposites, Adv Mat Res 910 (2014) 153–156, https://doi.org/10.4028/www.scientific.net/AMR.910.153.
[60] A.E. Patterson, T.R. Pereira, J.T. Allison, S.L. Messimer, IZOD impact properties of full-density fused deposition modeling polymer materials with respect to raster angle and print orientation, Proc. Inst. Mech. Eng. Part C J Mech Eng Sci (2019) 1–18, https://doi.org/10.1177/0954406219840385.